

Decoupled Charged Anisotropic Spherical Solutions in Rastall Gravity

M. Sharif¹ * and M. Sallah^{1,2} †

¹ Department of Mathematics and Statistics, The University of Lahore
1-KM Defence Road Lahore-54000, Pakistan.

² Department of Mathematics, The University of The Gambia,
Serrekunda, P.O. Box 3530, The Gambia.

Abstract

This paper uses the gravitational decoupling through the minimal geometric deformation approach and extends a known isotropic solution for a self-gravitating interior to two types of anisotropic spherical solutions in Rastall gravity in the presence of electromagnetic field. By deforming only the radial metric component, the field equations are decoupled into two sets, the first of which corresponds to an isotropic distribution of matter while the second set contains the anisotropic source. We obtain a solution of the first set by employing the charged isotropic Finch-Skea ansatz, whereas a solution for the second set is obtained by adopting two mimic constraints on the pressure and density. The matching conditions at the stellar surface are explored with the exterior geometry given by the deformed Reissner-Nordstrom space-time. For the two fixed values of the Rastall and charge parameters, we investigate physical features of both solutions through graphical analysis of the energy conditions, equation of state parameters, surface redshift and compactness function. The stability of both solutions is also studied through the Herrera cracking approach and causality condition. We deduce that while both solutions are physically viable, only the solution corresponding to the pressure-like constraint is stable.

*msharif.math@pu.edu.pk

†malick.sallah@utg.edu.gm

Keywords: Rastall gravity; Anisotropy; Gravitational decoupling; Self-gravitating systems.

PACS: 04.50.Kd; 04.40.Dg; 04.40.-b.

1 Introduction

General Relativity (GR) is regarded as one of the most important pillars for comprehending the underlying notions of gravitational phenomena and cosmology. Several cosmological measurements indicate that celestial objects are not randomly distributed in the universe but are instead systematically ordered. The study of such interstellar objects and their physical attributes encourage us to figure out cosmic expansion. This expansion is thought to be carried out by an obscure type of energy known as dark energy which has a repulsive tendency. Through the introduction of the cosmological constant, an attempt has been made in GR to explain the nature and gravitational effects of dark energy. However, several researchers have argued the limitations/deficiency of the cosmological constant in explaining the true dynamics of dark energy. To this end, modified gravity theories were proposed. One such modified theory is the Rastall gravity theory, proposed by Rastall in 1972 [1]. According to this theory, the stress-energy tensor which exhibits null divergence in flat spacetime is not necessarily conserved in curved spacetime geometry. Rastall gravity differs from GR in that it includes the Ricci scalar through the Rastall parameter. Despite being manually introduced, this factor alters not only the field equations but also the way material fields are linked to the gravitational interaction.

The minimal coupling concept clearly does not apply in this theory. This, however, brings with it new and interesting ideas that may help us to understand a variety of well studied phenomena, including cosmological challenges, stellar systems, collapsed structures such as black holes, gravitational waves and so on. Rastall gravity is thus competitive with other modified theories of gravity such as $f(\mathcal{R})$ and $f(\mathcal{R}, T)$ theories, where \mathcal{R} and T are the Ricci scalar and trace of the stress-energy tensor, respectively. An important feature of the Rastall theory is that from the geometric perspective, any perfect fluid solution of the Einstein field equations is also a solution of the Rastall field equations. Furthermore, both GR and Rastall gravity have the same vacuum solution with respect to black holes. The Rastall field equations do not have an accompanying Lagrangian density from which they can be calcu-

lated, but nevertheless, generalize the GR field equations whilst maintaining the general coordinate transformation of the theory.

The complex nature of the self-gravitating bodies is made clear by the analytical solutions to the field equations. However, because the field equations are non-linear, it is frequently challenging to find solutions. A recently developed method to find workable solutions is the gravitational decoupling by minimal geometric deformation (MGD). In this method, the system of field equations is divided into two sets by means of a linear transformation that distorts the radial function of the line element. The extra source is represented by the second set, while the first set describes the seed sector. These two sets are treated separately, and the superposition principle is used to get the solution for the entire system. The MGD has its origins in the brane-world theory [2] and in [3], which were then expanded upon to look into new black hole solutions [4, 5]. An exact interior solution for isotropic spherically symmetric compact distributions was created by Ovalle and Linares [6]. This solution is essentially a brane-world adaption of Tolman's solution.

In order to modify the temporal and radial metric functions of spherical self-gravitating systems with a naked singularity at the Schwarzschild radius, Casadio et al. [7] reported a unique external solution. Using the same method, Ovalle [8] went on to construct anisotropic solutions from ideal fluid configurations with spherical symmetry. Isotropic interior solutions were extended by Ovalle et al. [9] to account for anisotropy. In an effort to develop anisotropic solutions from known isotropic domains in Rastall gravity and other modified theories, Maurya and his associates [10]-[15] worked on the MGD technique. From a known isotropic solution, Sharif and Saba [16]-[18] developed charged/uncharged gravitational decoupled anisotropic solutions and assessed the stability and sustainability of the resultant solutions within the context of $f(G)$ gravity (G is the Gauss-Bonnet invariant). In order to verify the viability of compact stars in the framework of various modified theories, numerous researchers obtained anisotropic versions of the isotropic source [19]-[22].

The participation of the electromagnetic field in celestial formations has an intriguing effect on how their evolution can be researched and examined. The impact of charge on stellar bodies in GR has been extensively studied through a vast corpus of literature and updated models. A static sphere that constitutes a charged perfect fluid was discussed by Xingxiang [23]. By matching the outer Reissner-Nordstrom (RN) metric with the inner geometry, Das et al. [24] investigated charged static spherical solutions. The field

equations for a shearfree charged object were numerically solved by Sharif and Bhatti [25], who also verified the solution's feasibility using the energy conditions. Murad [26] investigated anisotropic charged celestial objects with the assumption of a particular metric potential. In the presence of an electric field, many features characterizing the internal composition of self-gravitating entities have been investigated [27]-[29]. Using the Krori-Barua spacetime and the MGD method, Sharif and Sadiq [30] investigated the effect of charge and created two anisotropic solutions. In $f(\mathcal{R}, T, R_{\gamma\nu}T^{\gamma\nu})$ gravity, Sharif and Naseer [31, 32] obtained charged as well as uncharged anisotropic spherical solutions by minimally deforming the Krori-Barua ansatz. Sharif and Hassan [33, 34] also obtained charged-uncharged anisotropic spherical solutions in the context of $f(G, T)$ gravity using the MGD approach.

In addition to providing insights into useful astrophysical phenomena, some researchers [35] were able to obtain precise solutions by accounting for a certain sort of anisotropy. This allowed them to demonstrate that spherical stars may sustain positive and finite pressures and densities. Gleiser and Dev [36] demonstrated that anisotropy can sustain stars with a specific compactness $\frac{M}{2R} = \frac{2}{9}$ (M and R denote mass and radius, respectively) and concluded that stable configurations exist for specific adiabatic index relative to isotropic fluids. By attaining precise solutions for spherically symmetric anisotropic matter distributions with a linear equation of state (EoS), Sharma and Maharaj [37] made significant advancements in the modeling of compact stars. As part of his investigation on the stability of self-gravitating models, Herrera [38] proposed the concepts of cracking and overturning to examine the behavior of isotropic and anisotropic structures following perturbations. His findings showed that perfect fluid distributions are stable while anisotropic fluid distributions fracture. By adding sound speed, Abreu et al. [39] expanded the concept of cracking to study anisotropic spherical structures. They concluded that when the square of the tangential sound speed is greater than the square of the radial sound speed, the system becomes unstable.

This paper examines the relationship between Rastall gravity and charged anisotropic spherical systems in an effort to create solutions that appropriately capture the gravitational behavior of self-gravitating systems. The rest of the paper is structured as follows. Effective parameters are determined by analyzing the Rastall field equations for a static spherically symmetric matter distribution in section 2. In section 3, we split the Rastall field equations into two workable sets using the MGD technique. The matching conditions

at the stellar surface are also examined. In section 4, by extending a known charged perfect fluid ansatz, we obtain two solutions for anisotropic spherical source. We examine physical properties spanning from the viability to stability of our acquired solutions. Finally, section 5 discusses a summary of our findings.

2 Rastall Gravity Theory

The Rastall gravity theory arose as a result of the rejection of the fundamental premise that the stress-energy tensor freely diverges in a curved spacetime. The Rastall field equations, given by

$$R_{\gamma\varrho} - \frac{1}{2}\mathcal{R}g_{\gamma\varrho} = \kappa(T_{\gamma\varrho}^{(m)} - \lambda\mathcal{R}g_{\gamma\varrho}), \quad (1)$$

are consistent with the assumption that

$$\nabla_{\varrho}T^{\gamma\varrho} = \lambda g^{\gamma\varrho}\nabla_{\varrho}\mathcal{R}, \quad (2)$$

and reduce to the Einstein's field equations in the event $\lambda = 0$. The non-conservation of the stress-energy tensor (2) as proposed by Rastall, induces a non-minimal coupling between matter and geometry. In the preceding equations, κ is the coupling constant and λ is the Rastall parameter that causes the deviation from GR and by which the Ricci scalar is non-minimally coupled into the theory. The term $T_{\gamma\varrho}^{(m)}$ denotes a charged perfect fluid matter configuration given by

$$T_{\gamma\varrho}^{(m)} = (\rho + P)u_{\gamma}u_{\varrho} - P g_{\gamma\varrho} + \frac{1}{4\pi}\left[\frac{1}{4}g_{\gamma\varrho}F^{\tau\nu}F_{\tau\nu} - F_{\gamma}^{\tau}F_{\varrho\tau}\right], \quad (3)$$

where $u^{\gamma} = e^{-\frac{\beta(r)}{2}}\delta_0^{\gamma}$ is the fluid 4-velocity while ρ and P represent the energy density and isotropic pressure, respectively. The term $F_{\gamma\varrho} = \alpha_{\varrho,\gamma} - \alpha_{\gamma,\varrho}$ denotes the Maxwell field tensor with $\alpha_{\varrho} = \alpha(r)\delta_{\varrho}^0$ as 4-potential. This Maxwell tensor satisfies the Maxwell field equations given by

$$F_{;\varrho}^{\gamma\varrho} = 4\pi J^{\gamma}, \quad F_{[\gamma\varrho;\eta]}, \quad (4)$$

where J^{γ} is the 4-current which can be written in terms of charged density ζ as $J^{\gamma} = \zeta(r)u^{\gamma}$.

For the purpose of describing our interior geometry, we shall consider a static spherically symmetric spacetime in Schwarzschild-like coordinates as

$$ds_-^2 = e^{\beta(r)} dt^2 - e^{\eta(r)} dr^2 - r^2(d\theta^2 + \sin^2\theta d\phi^2), \quad (5)$$

where the areal radius r ranges from the stars center ($r = 0$) to an arbitrary point ($r = R$) on the surface of the star. The Maxwell field equation for our spacetime becomes

$$\alpha'' + \left(\frac{2}{r} - \frac{\beta'}{2} - \frac{\eta'}{2} \right) \alpha' = 4\pi\zeta e^{\frac{\beta}{2} + \eta}, \quad (6)$$

where $' = \frac{\partial}{\partial r}$. Upon integration of the above equation, we have

$$\alpha' = \frac{e^{\frac{\beta+\eta}{2}} q(r)}{r^2}, \quad (7)$$

$q(r) = 4\pi \int_0^r \zeta e^{\frac{\eta}{2}} r^2 dr$ indicates the total charge in the interior of the sphere. By defining

$$\bar{T}_{\gamma\varrho}^{(eff)} = T_{\gamma\varrho}^{(m)} - \lambda \mathcal{R} g_{\gamma\varrho}, \quad (8)$$

we can rewrite the field equations (1) as

$$G_{\gamma\varrho} = \kappa \bar{T}_{\gamma\varrho}^{(eff)}. \quad (9)$$

This shows that the original Rastall field equations can always be restructured to remold the Einstein's field equations, thereby regaining the standard result $\nabla_\varrho \bar{T}^{\gamma\varrho(eff)} = 0$. This rearrangement can also be performed in other modified gravity theories such as $f(\mathcal{R})$, $f(\mathcal{R}, T)$ theories among others, irrespective of the conservation of the stress-energy tensor.

Upon contracting the field equations (1), we can write the Ricci scalar as

$$\mathcal{R} = \frac{\kappa T}{4\lambda\kappa - 1}, \quad (10)$$

which can, in turn, be used to rewrite the effective stress-energy tensor (8) as

$$\bar{T}_{\gamma\varrho}^{(eff)} = T_{\gamma\varrho}^{(m)} - \frac{\varepsilon T}{4\varepsilon - 1} g_{\gamma\varrho}, \quad (11)$$

where $\varepsilon = \lambda\kappa$. We shall proceed with the assumption that $\kappa = 1$ so that $\varepsilon = \lambda$. At this point, it is clear that $\lambda = \frac{1}{4}$ depicts a non-realistic scenario

and must therefore be avoided. The components of the effective stress-energy tensor (11) are thus obtained as

$$\bar{T}_{00}^{(eff)} = g_{00} \left(\frac{3\lambda(\rho + P) - \rho}{4\lambda - 1} \right) + g_{00} \left(\frac{q^2}{8\pi r^4} \right), \quad (12)$$

$$\bar{T}_{11}^{(eff)} = -g_{11} \left(\frac{\lambda(\rho + P) - P}{4\lambda - 1} \right) + g_{11} \left(\frac{q^2}{8\pi r^4} \right), \quad (13)$$

$$\bar{T}_{22}^{(eff)} = -g_{22} \left(\frac{\lambda(\rho + P) - P}{4\lambda - 1} \right) - g_{22} \left(\frac{q^2}{8\pi r^4} \right). \quad (14)$$

We now shift our attention to the field equations for multiple matter sources, given by

$$R_{\gamma\varrho} - \frac{1}{2} \mathcal{R} g_{\gamma\varrho} = T_{\gamma\varrho}^{(tot)}, \quad (15)$$

with

$$T_{\gamma\varrho}^{(tot)} = \bar{T}_{\gamma\varrho}^{(eff)} + \delta \Theta_{\gamma\varrho}. \quad (16)$$

Here, $\bar{T}_{\gamma\varrho}^{(eff)}$ is the effective energy-momentum tensor given by Eq.(8) and the term $\Theta_{\gamma\varrho}$ is an additional source gravitationally coupled to the seed source through the decoupling constant δ , that may generate anisotropy in self-gravitating fields.

New fields such as scalar, tensor and vector fields may well be contained in the source $\Theta_{\gamma\varrho}$. By virtue of its definition, the total energy-momentum tensor in (16) must now satisfy the conservation equation given by

$$T_{\varrho}^{\gamma}{}_{;\gamma} = 0. \quad (17)$$

The corresponding Rastall field equations turn out to

$$e^{-\eta} \left(\frac{\eta'}{r} - \frac{1}{r^2} \right) + \frac{1}{r^2} = \frac{3\lambda(\rho + P) - \rho}{4\lambda - 1} + \frac{q^2}{8\pi r^4} + \delta \Theta_0^0, \quad (18)$$

$$e^{-\eta} \left(\frac{\beta'}{r} + \frac{1}{r^2} \right) - \frac{1}{r^2} = \frac{\lambda(\rho + P) - P}{4\lambda - 1} - \frac{q^2}{8\pi r^4} - \delta \Theta_1^1, \quad (19)$$

$$e^{-\eta} \left(\frac{\beta''}{2} + \frac{\beta'^2}{4} - \frac{\beta'\eta'}{4} + \frac{\beta' - \eta'}{2r} \right) = \frac{\lambda(\rho + P) - P}{4\lambda - 1} + \frac{q^2}{8\pi r^4} - \delta \Theta_2^2. \quad (20)$$

With respect to the system (18) - (20), the conservation equation in (17) now reads

$$\bar{P}'(r) + \frac{\beta'(r)}{2} (\bar{\rho} + \bar{P}) + \frac{2\delta}{r} (\Theta_2^2 - \Theta_1^1) + \frac{\delta\beta'(r)}{2} (\Theta_0^0 - \Theta_1^1) - \delta \left(\Theta_1^1(r) \right)' - \frac{qq'}{4\pi r^4} = 0, \quad (21)$$

where $\bar{\rho} = \frac{3\lambda(\rho+P)-\rho}{4\lambda-1}$ and $\bar{P} = \frac{\lambda(\rho+P)-P}{4\lambda-1}$. Equations (18)-(21) constitute four non-linear differential equations with eight unknowns given by $(\beta, \eta, \rho, P, q, \Theta_0^0, \Theta_1^1, \Theta_2^2)$. From this system, we identify three effective matter components given by

$$\rho^{eff} = \rho + \delta \Theta_0^0, \quad \bar{P}_r^{eff} = P - \delta \Theta_1^1, \quad \bar{P}_t^{eff} = P - \delta \Theta_2^2. \quad (22)$$

These definitions of the effective parameters indicate that the source $\Theta_{\gamma\varrho}$ can induce an anisotropy within the stellar distribution given by

$$\bar{\Delta}^{eff} = P_t^{(eff)}(r) - P_r^{(eff)}(r) = \delta (\Theta_1^1 - \Theta_2^2). \quad (23)$$

In what follows, we explore the MGD technique in a bid to solve the field equations (18)-(20).

3 Decoupling with MGD

In order to find a solution to the field equations (18)-(20), we apply the gravitational decoupling procedure with the MGD approach. Via this approach, the system will be modified in such a way that the field equations associated with the extra source $\Theta_{\gamma\varrho}$ assume the form of the effective quasi Einstein equations. To proceed, we assume a charged perfect fluid solution (ξ, χ, ρ, P, q) described by the line element

$$ds^2 = e^{\xi(r)} - \frac{dr^2}{\chi(r)} - r^2(d\theta^2 + \sin^2 \theta d\phi^2), \quad (24)$$

where $\chi(r) = 1 - \frac{2m}{r} + \frac{q^2}{r^2}$, m denotes the Misner-Sharp mass of the stellar object with perfect matter configuration. To introduce the effects of the source $\Theta_{\gamma\varrho}$ on charged isotropic solution, we consider the following linear transformations on the metric components

$$\xi(r) \mapsto \beta(r) = \xi(r), \quad \chi(r) \mapsto e^{-\eta(r)} = \chi(r) + \delta g^*(r), \quad (25)$$

where g^* is the deformation associated with the radial component of the metric function. It can be observed that the MGD approach only acts on the radial component of the metric and leaves the temporal metric component un-deformed. By substituting the deformed radial coefficient in the field

Eqs.(18)-(20), two sets of differential equations are obtained. The first set corresponds to a perfect fluid configuration with $\delta = 0$ and reads

$$\frac{1}{r^2} - \frac{\chi}{r^2} - \frac{\chi'}{r} = \frac{3\lambda(\rho + P) - \rho}{4\lambda - 1} + \frac{q^2}{8\pi r^4}, \quad (26)$$

$$\chi\left(\frac{\beta'}{r} + \frac{1}{r^2}\right) - \frac{1}{r^2} = \frac{\lambda(\rho + P) - P}{4\lambda - 1} - \frac{q^2}{8\pi r^4}, \quad (27)$$

$$\chi\left(\frac{\beta''}{2} + \frac{\beta'^2}{4} + \frac{\beta'}{2r}\right) + \chi'\left(\frac{\beta'}{4} + \frac{1}{2r}\right) = \frac{\lambda(\rho + P) - P}{4\lambda - 1} + \frac{q^2}{8\pi r^4}, \quad (28)$$

with the associated conservation equation

$$\bar{P}'(r) + \frac{\beta'(r)}{2}(\bar{\rho} + \bar{P}) - \frac{qq'}{4\pi r^4} = 0. \quad (29)$$

The second set of equations entails the source $\Theta_{\gamma\ell}$ given by

$$\Theta_0^0 = -\frac{g^{*'}}{r} - \frac{g^*}{r^2}, \quad (30)$$

$$\Theta_1^1 = -g^*\left(\frac{\beta'}{r} + \frac{1}{r^2}\right), \quad (31)$$

$$\Theta_2^2 = -g^*\left(\frac{\beta''}{2} + \frac{\beta'^2}{4} + \frac{\beta'}{2r}\right) - g^{*'}\left(\frac{\beta'}{4} + \frac{1}{2r}\right), \quad (32)$$

and satisfies the conservation equation

$$\frac{2}{r}(\Theta_2^2 - \Theta_1^1) + \frac{\alpha'(r)}{2}(\Theta_0^0 - \Theta_1^1) - \left(\Theta_1^1(r)\right)' = 0. \quad (33)$$

The system given by Eqs.(30)-(32) resembles the field equations for the anisotropic spherically symmetric matter configuration with effective parameters $\rho^{eff} = \Theta_0^0$, $P_r^{eff} = -\Theta_1^1$, $P_t^{eff} = -\Theta_2^2$, and the corresponding metric becomes

$$ds^2 = e^{\beta(r)} dt^2 - \frac{dr^2}{g^*(r)} - r^2(d\theta^2 + \sin^2\theta d\phi^2).$$

However, due to a missing $\frac{1}{r^2}$ term in the right hand side of the first two equations, this system does not represent typical field equations for anisotropic matter configuration. The matter components thus become

$$\rho^{eff} + \frac{q^2}{8\pi r^4} = \Theta_0^{*0} = \Theta_0^0 + \frac{1}{r^2},$$

$$P_r^{eff} - \frac{q^2}{8\pi r^4} = \Theta_1^{*1} = \Theta_1^1 + \frac{1}{r^2},$$

$$P_t^{eff} + \frac{q^2}{8\pi r^4} = \Theta_2^{*2} = \Theta_2^2 = \Theta_3^{*3} = \Theta_3^3.$$

We now shift our attention to the junction conditions which provide the governing rules for the smooth matching of the interior and exterior space-time geometries at the surface of the star (where $r = R$). Our interior spacetime geometry is given by the deformed metric

$$ds_-^2 = e^{\beta(r)} dt^2 - \frac{1}{\left(1 - \frac{2m(r)}{r} + \delta g^*(r) + \frac{q^2}{r^2}\right)} dr^2 - r^2(d\theta^2 + \sin^2 \theta d\phi^2), \quad (34)$$

which is to be matched with the general outer metric given by

$$ds_+^2 = e^{\beta(r)} dt^2 - e^{\eta(r)} dr^2 - r^2(d\theta^2 + \sin^2 \theta d\phi^2). \quad (35)$$

Hence, the continuity of the first fundamental form ($[ds^2]_\Sigma = 0$) of junction conditions at the hypersurface Σ yields

$$\beta(R)_- = \beta(R)_+, \quad (36)$$

and

$$1 - \frac{2M_0}{R} + \frac{Q_0^2}{R^2} + \delta g_R^* = e^{-\eta(R)_+}, \quad (37)$$

where $\chi = e^{-\eta} - \delta g^*$. Also, $M_0 = m(R)$, $Q_0^2 = q^2(R)$ and g_R^* denote the mass, charge and deformation at the surface of the star.

Similarly, the continuity of the second fundamental form ($[T_{\gamma^\varrho}, S^\varrho]_\Sigma = 0$, S^ϱ denotes a unit 4-vector) gives

$$P(R) - \frac{Q_0^2}{8\pi R^4} - \delta (\Theta_1^1(R))_- = -\delta (\Theta_1^1(R))_+. \quad (38)$$

Substituting Eq.(31) for the interior geometry in (38) yields

$$P(R) - \frac{Q_0^2}{8\pi R^4} + \delta g^*(R) \left(\frac{\beta'(R)}{R} + \frac{1}{R^2} \right) = -\delta (\Theta_1^1(R))_+. \quad (39)$$

Using Eq.(31) for the outer geometry in (39), we obtain

$$P(R) - \frac{Q_0^2}{8\pi R^4} + \delta g^*(R) \left(\frac{\beta'(R)}{R} + \frac{1}{R^2} \right) = \delta b^*(R) \left[\frac{1}{R^2} + \frac{2MR - 2Q^2}{R^2(R^2 - 2MR + Q^2)} \right], \quad (40)$$

where \mathcal{M} and \mathcal{Q} denote the mass and charge in the exterior region and $b^*(R)$ indicates the deformation on the outer RN solution by the source $\Theta_{\gamma\varrho}$, as shown below

$$ds^2 = \left(1 - \frac{2\mathcal{M}}{r} + \frac{\mathcal{Q}^2}{r^2}\right) dt^2 - \frac{1}{\left(1 - \frac{2\mathcal{M}}{r} + \frac{\mathcal{Q}^2}{r^2} + \delta b^*(r)\right)} dr^2 - r^2 d\Omega^2. \quad (41)$$

Equations (36), (37) and (40) are the necessary and sufficient conditions for the smooth matching of the deformed interior metric (34) and the deformed RN metric (41).

4 Anisotropic Solutions

Here, we obtain charged anisotropic spherical solutions for compact stellar configuration by assuming a charged isotropic seed solution of the field equations (18)-(20). For this purpose, we adopt the charged Finch-Skea solution due to its non-singularity and physical plausibility. The solution is given by [40]

$$e^{\beta(r)} = \left[A + \frac{1}{2}Br\sqrt{Cr^2}\right]^2, \quad (42)$$

$$\chi(r) = \frac{1}{1 + Cr^2}, \quad (43)$$

$$\begin{aligned} \rho = & \frac{-C}{2\sqrt{Cr^2}(Cr^2 + 1)^2 \left(2A + Br\sqrt{Cr^2}\right)^2} \left[4A^2\sqrt{Cr^2} \left(C(4\lambda - 1)r^2 \right. \right. \\ & + \left. 12\lambda - 6 \right) - 2Br \ln \left(A + \frac{1}{2}Br\sqrt{Cr^2} \right) \left(2B(4\lambda - 1)r\sqrt{Cr^2} (Cr^2 + 1) \right. \\ & \times \left. \ln \left(A + \frac{1}{2}Br\sqrt{Cr^2} \right) + 2A (C(8\lambda + 1)r^2 + 12\lambda) + Br\sqrt{Cr^2} \right. \\ & \times \left. \left(3Cr^2 + 4\lambda + 2 \right) \right) + 4ABCr^3 (C(4\lambda - 1)r^2 + 12\lambda - 6) \\ & + \left. B^2r^2\sqrt{Cr^2} (Cr^2 (C(4\lambda - 1)r^2 - 4\lambda - 2) - 16\lambda + 4) \right], \quad (44) \end{aligned}$$

$$P = \frac{C}{2\sqrt{Cr^2}(Cr^2 + 1)^2 \left(2A + Br\sqrt{Cr^2}\right)^2} \left[4A^2\sqrt{Cr^2} \left(C(4\lambda - 1)r^2 \right. \right.$$

$$\begin{aligned}
& + 12\lambda - 2 \Big) + 2Br \ln \left(A + \frac{1}{2}Br\sqrt{Cr^2} \right) \left(-2B(4\lambda - 1)r\sqrt{Cr^2} \right. \\
& \times (Cr^2 + 1) \ln \left(A + \frac{1}{2}Br\sqrt{Cr^2} \right) + A(2C(3 - 8\lambda)r^2 - 24\lambda + 8) \\
& + Br\sqrt{Cr^2}(Cr^2 - 4\lambda + 2) \Big) + 4ABCr^3(C(4\lambda - 1)r^2 + 12\lambda - 2) \\
& + B^2r^2\sqrt{Cr^2}(Cr^2(C(4\lambda - 1)r^2 - 4\lambda + 2) - 16\lambda + 4) \Big], \quad (45) \\
q^2 &= \frac{4\pi Cr^5}{(Cr^2 + 1)^2 \left(2A + Br\sqrt{Cr^2} \right)^2} \left[r \left(4A^2C + 4ABCr\sqrt{Cr^2} + B^2 \right. \right. \\
& \times (Cr^2 + 2)^2 \Big) + 2B \ln \left(A + \frac{1}{2}Br\sqrt{Cr^2} \right) \left(4Br(Cr^2 + 1) \right. \\
& \times \ln \left(A + \frac{1}{2}Br\sqrt{Cr^2} \right) - 2A\sqrt{Cr^2} - Br(3Cr^2 + 2) \Big) \Big], \quad (46)
\end{aligned}$$

where the constants A , B and C can be determined from the matching conditions. With the RN metric as our exterior spacetime, the matching conditions yield

$$\begin{aligned}
A &= \sqrt{\frac{R^2 - 2M_0R + Q_0^2}{R^2}} - \frac{M_0R - Q_0^2}{2R\sqrt{R^2 - 2M_0R + Q_0^2}}, \\
B &= \frac{MR - Q_0^2}{R^2\sqrt{2M_0R - Q_0^2}}, \quad C = \frac{1}{R^2 - 2M_0R + Q_0^2} - \frac{1}{R^2}, \quad (47)
\end{aligned}$$

with the compactness $\frac{M_0}{2R} < \frac{2}{9}$. These values ensure the surface continuity of the interior and exterior geometries and will most certainly be altered upon addition of the source Θ_{γ_ℓ} . We now find anisotropic solutions by setting $\delta \neq 0$ in the interior geometry and utilize Eqs.(42) and (43) as our temporal and radial metric coefficients, respectively. The deformation function $g^*(r)$ is related to the source Θ_{γ_ℓ} through Eqs.(30)-(32), which is a system of three equations in four unknowns. It thus suffices to impose a single constraint to close this system. In what follows, we obtain two anisotropic solutions by imposing a single constraint in each case.

4.1 Solution I

We impose a constraint on Θ_1^1 and obtain a solution of the field Eqs.(30)-(32) for g^* and $\Theta_{\gamma\varrho}$. The interior geometry is compatible with the exterior spacetime (given by the RN metric) whenever $P(R) - \frac{Q_0^2}{8\pi R^4} \sim \delta(\Theta_1^1(R))_-$, leading to the simplest choice

$$P - \frac{q^2}{8\pi r^4} = \Theta_1^1. \quad (48)$$

From the equation above, we obtain an explicit expression for the deformation function given by

$$\begin{aligned} g^*(r) = & \frac{-Cr^2}{(Cr^2 + 1)^2 \left[BCr^3 \left(4 \ln \left(A + \frac{1}{2} Br \sqrt{Cr^2} \right) + 1 \right) + 2A \sqrt{Cr^2} \right]} \\ & \times \frac{1}{\left(2A + Br \sqrt{Cr^2} \right)} \left[4A^2 \sqrt{Cr^2} (C(2\lambda - 1)r^2 + 6\lambda - 1) - 2Br \right. \\ & \times \ln \left(A + \frac{1}{2} Br \sqrt{Cr^2} \right) \left(B(4\lambda + 1)r \sqrt{Cr^2} (Cr^2 + 1) \right. \\ & \times \ln \left(A + \frac{1}{2} Br \sqrt{Cr^2} \right) + 4A (C(2\lambda - 1)r^2 + 3\lambda - 1) \\ & \left. \left. + 2Br \sqrt{Cr^2} (-Cr^2 + \lambda - 1) \right) + 4ABCr^3 (C(2\lambda - 1)r^2 + 6\lambda - 1) \right. \\ & \left. \left. + B^2 r^2 \sqrt{Cr^2} (Cr^2 (C(2\lambda - 1)r^2 - 2\lambda - 1) - 8\lambda) \right] \right]. \quad (49) \end{aligned}$$

Using the above equation, we can obtain an expression for the radial metric function defined in Eq.(25) as

$$\begin{aligned} e^{-\eta(r)} = & \frac{-C\delta r^2}{(Cr^2 + 1)^2 \left(BCr^3 \left(4 \ln \left(A + \frac{1}{2} Br \sqrt{Cr^2} \right) + 1 \right) + 2A \sqrt{Cr^2} \right)} \\ & \times \frac{1}{\left(2A + Br \sqrt{Cr^2} \right)} \left[4A^2 \sqrt{Cr^2} (C(2\lambda - 1)r^2 + 6\lambda - 1) - 2Br \right. \\ & \times \ln \left(A + \frac{1}{2} Br \sqrt{Cr^2} \right) \left(B(4\lambda + 1)r \sqrt{Cr^2} (Cr^2 + 1) \ln \left(A \right. \right. \end{aligned}$$

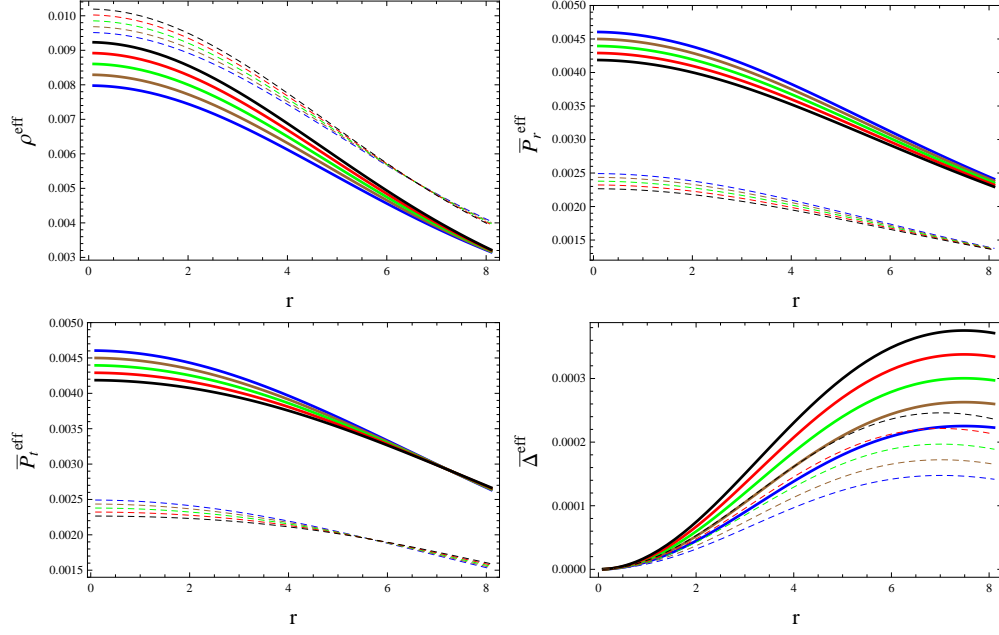


Figure 1: Plots of ρ^{eff} , \bar{P}_r^{eff} , \bar{P}_t^{eff} and $\bar{\Delta}^{eff}$ versus r corresponding to $\lambda = 0.3$ (solid), 0.25 (dashed), $\delta = 0.12$ (blue), 0.14 (brown), 0.16 (green), 0.18 (red), 0.2 (black) and $Q_0 = 0.01$ for solution I.

$$\begin{aligned}
& + \frac{1}{2}Br\sqrt{Cr^2} \Big) + 4A \left(C(2\lambda - 1)r^2 + 3\lambda - 1 \right) + 2Br\sqrt{Cr^2} \left(\lambda - 1 \right. \\
& \left. - Cr^2 \right) \Big) + 4ABCr^3 \left(C(2\lambda - 1)r^2 + 6\lambda - 1 \right) + B^2r^2\sqrt{Cr^2} \left(Cr^2 \right. \\
& \left. \times \left(C(2\lambda - 1)r^2 - 2\lambda - 1 \right) - 8\lambda \right) \Big] + \frac{1}{Cr^2 + 1} . \tag{50}
\end{aligned}$$

The interior metric functions (42) and (50) denote the minimally deformed Finch-Skea solution. The expressions for the effective parameters together with the induced anisotropy are given in the Appendix. We now interpret this solution through graphical analysis of the effective parameters (ρ^{eff} , \bar{P}_r^{eff} , \bar{P}_t^{eff}) and the anisotropy, $\bar{\Delta}^{eff}$. We have done this analysis for the star Her X-1 with mass $M_0 = 0.85M_\odot$ and radius $R = 8.1km$ [41]. Throughout this analysis, we have used two values of the Rastall parameter and charge parameter given by $\lambda = 0.3, 0.25$ and $Q_0 = 0.01, 2$ respectively, with the decoupling constant as $\delta = 1.2, 1.4, 1.6, 1.8, 2$. The values used for these

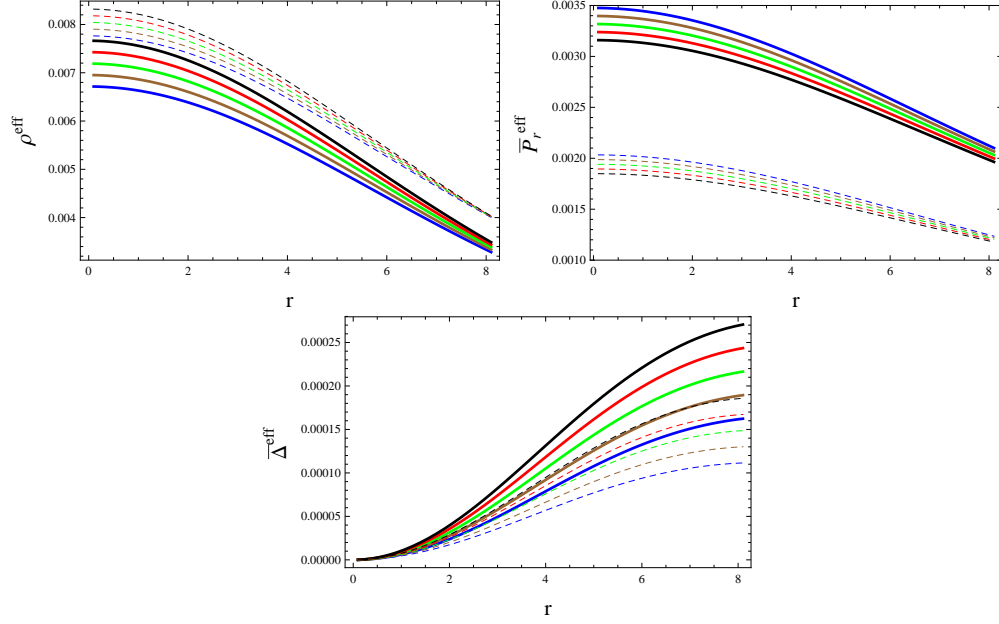


Figure 2: Plots of ρ^{eff} , \bar{P}_r^{eff} , \bar{P}_t^{eff} and $\bar{\Delta}^{\text{eff}}$ versus r corresponding to $\lambda = 0.3$ (solid), 0.25 (dashed), $\delta = 0.12$ (blue), 0.14 (brown), 0.16 (green), 0.18 (red), 0.2 (black) and $Q_0 = 2$ for solution I.

parameters have been selected after a long trial for which they have been found to induce the desired behavior in the obtained model. We see that the behavior of the effective parameters (density, radial and tangential pressures) is consistent with the behavior of compact objects, i.e., finite, positive and maximum at the core and monotonically decreasing towards the surface of the star. This is shown in Figures 1 and 2.

It can be observed from both figures that the density incurs higher values for $\lambda = 0.25$ when compared to $\lambda = 0.3$. This leads to the conclusion that a reduction in the Rastall parameter renders a more dense interior of compact stars. The effect of the decrement in the Rastall parameter is seen to correspond to lower values of the radial and tangential pressures. Furthermore, the radial and tangential pressures reach the same magnitude near the core, causing an anisotropy that disappears at that point and increases towards the surface. This positive anisotropy illustrates an outward directed pressure, leading to the anti-gravitational force which helps in the stability of compact structure. An increase in the Rastall parameter results in more

anisotropy. With regards to the charge, however, we observe that a higher value induces a less dense interior for compact objects. Figures 1 and 2 show that the effective parameters as well as anisotropy are slightly lowered by an increase in charge.

4.2 Solution II

We now adopt a density-like constraint for the purpose of obtaining a new charged anisotropic solution. This constraint is given by

$$\Theta_0^0(r) = \rho(r). \quad (51)$$

Using Eqs.(30) and (44) in the constraint above, we have

$$\begin{aligned} \frac{g^{*'}}{r} + \frac{g^*}{r^2} = & \frac{C}{2\sqrt{Cr^2}(Cr^2+1)^2(2A+Br\sqrt{Cr^2})^2} \left[4A^2\sqrt{Cr^2} \left(C(4\lambda-1)r^2 \right. \right. \\ & + 12\lambda - 6 \Big) + 4ABCr^3 \left(C(4\lambda-1)r^2 + 12\lambda - 6 \right) + B^2r^2\sqrt{Cr^2} \\ & \times \left(Cr^2 \left(C(4\lambda-1)r^2 - 4\lambda - 2 \right) - 16\lambda + 4 \right) - 2Br \ln \left(A + \frac{1}{2}Br \right. \\ & \times \sqrt{Cr^2} \Big) \left(2B(4\lambda-1)r\sqrt{Cr^2}(Cr^2+1) \log \left(A + \frac{1}{2}Br\sqrt{Cr^2} \right) \right. \\ & \left. \left. + 2A \left(C(8\lambda+1)r^2 + 12\lambda \right) + Br\sqrt{Cr^2}(3Cr^2+4\lambda+2) \right) \right]. \quad (52) \end{aligned}$$

Owing to the absence of an exact solution to the differential equation (52), we obtain a numerical approximation. Figures 3 and 4 show the plots of the effective parameters and anisotropy for this solution. For the graphical analysis, we have used the same values of the parameters as in solution I. It is seen from these figures that the effective parameters are finite and attain a positive as well as maximum value at the core whilst monotonically decreasing towards the boundary. It is also observed that lowering the value of the Rastall parameter enhances a denser interior of compact stars whilst inducing lower values for the radial and tangential pressures. The radial and tangential pressures attain almost similar values near the core thus inducing a positive anisotropy that vanishes near the core. With respect to the charge, it is observed that increasing its value enhances a less dense interior for

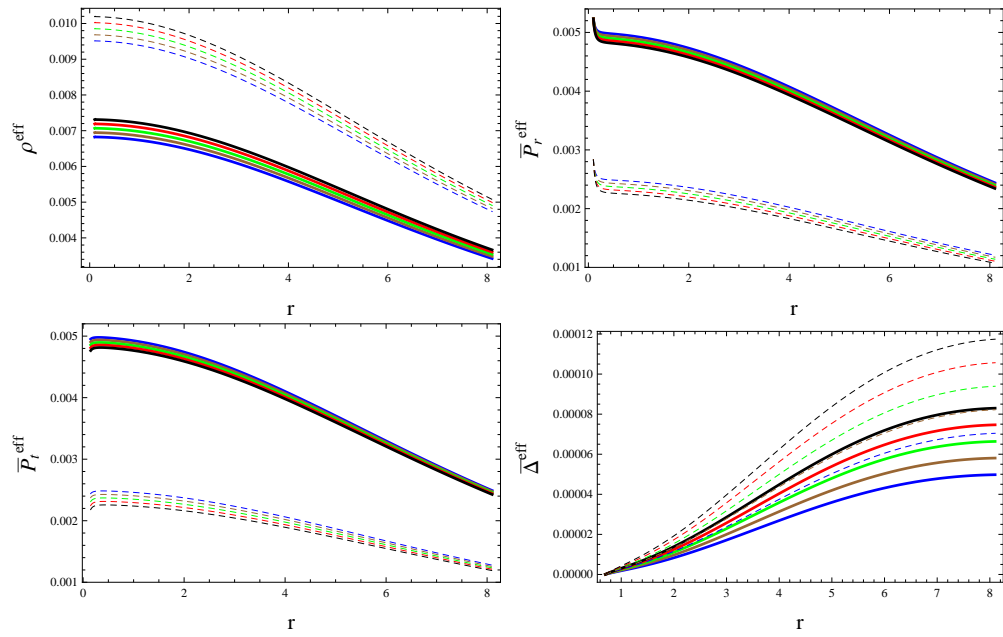


Figure 3: Plots of ρ^{eff} , \bar{P}_r^{eff} , \bar{P}_t^{eff} and $\bar{\Delta}^{eff}$ versus r corresponding to $\lambda = 0.3$ (solid), 0.25 (dashed), $\delta = 0.01$ (blue), 0.03 (brown), 0.05 (green), 0.07 (red), 0.09 (black) and $Q_0 = 0.01$ for solution II.

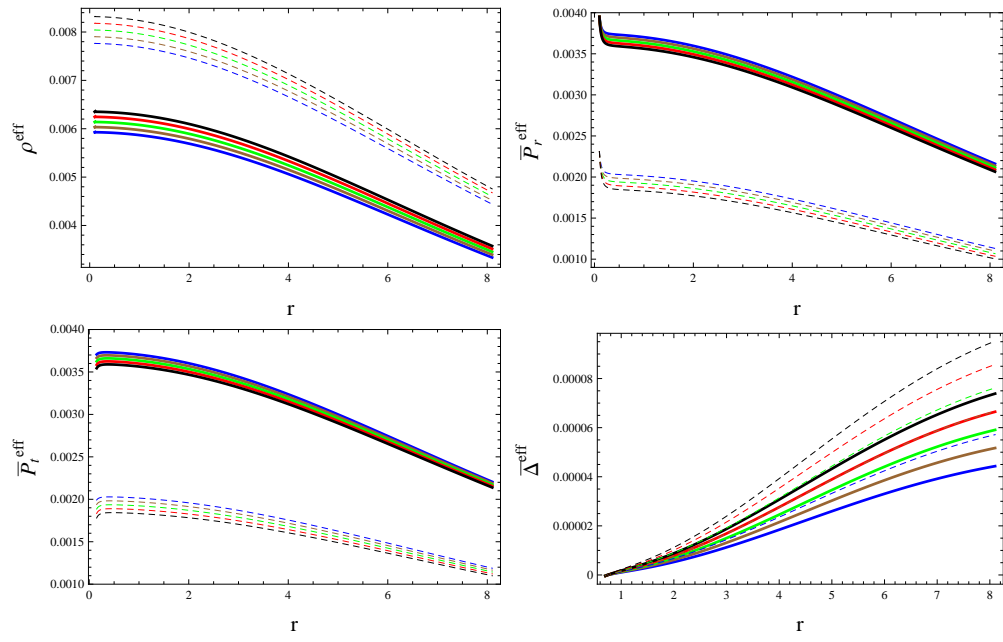


Figure 4: Plots of ρ^{eff} , \bar{P}_r^{eff} , \bar{P}_t^{eff} and $\bar{\Delta}^{\text{eff}}$ versus r corresponding to $\lambda = 0.3$ (solid), 0.25 (dashed), $\delta = 0.01$ (blue), 0.03 (brown), 0.05 (green), 0.07 (red), 0.09 (black) and $Q_0 = 2$ for solution II.

compact structures and lower values of radial and tangential pressures. A reduced anisotropy is also enhanced by an increase in charge. It is worthy to highlight that the alteration of the Rastall and charge parameters induces the same effects in both solutions I and II.

4.3 Physical Viability and Stability

Here, we investigate physical properties such as viability and stability of the obtained solutions. To study the physical viability, we explore the energy conditions. Through the energy conditions, we determine the presence of ordinary matter in the stellar interior. These conditions are bounds on the stress-energy tensor and are categorized as dominant, strong, weak and null energy conditions. For charged distribution of matter in Rastall theory, these conditions are given as

$$\begin{aligned}\rho^{eff} + \frac{q^2}{8\pi r^4} &\geq 0, & \rho^{eff} + \bar{P}_r^{eff} &\geq 0, \\ \rho^{eff} - \bar{P}_r^{eff} + \frac{q^2}{4\pi r^4} &\geq 0, & \rho^{eff} - \bar{P}_t^{eff} &\geq 0, \\ \rho^{eff} + \bar{P}_t^{eff} + \frac{q^2}{4\pi r^4} &\geq 0, & \rho^{eff} + \bar{P}_r^{eff} + 2\bar{P}_t^{eff} + \frac{q^2}{4\pi r^4} &\geq 0.\end{aligned}$$

Figures 5-8 show that these bounds are met by both solutions thus implying their physical viability. The radial and tangential EoS parameters given by $\omega_r = \frac{\bar{P}_r^{eff}}{\rho^{eff}}$ and $\omega_t = \frac{\bar{P}_t^{eff}}{\rho^{eff}}$, respectively, comprise an important component of self-gravitating objects and can be used to determine their physical viability. A necessary and sufficient condition for physical viability using the EoS parameters is that $0 \leq \omega_r \leq 1$ and $0 \leq \omega_t \leq 1$ [42]. These are shown in Figures 9 and 10 that depict the physical viability of both solutions.

For a static and spherically symmetric self-gravitating body, we determine the mass by the equation

$$m(r) = 4\pi \int_0^R \rho^{eff} r^2 dr. \quad (53)$$

With the initial condition $m(0) = 0$, the mass of anisotropic spherical structure can be numerically evaluated from the above equation. Using this mass, we can determine the compactness $u(r)$ and surface redshift $Z_s(r)$ defined by $u(r) = \frac{m(r)}{r}$ and $Z_s(r) = \frac{1}{\sqrt{1-2u(r)}} - 1$, respectively. For viable stellar

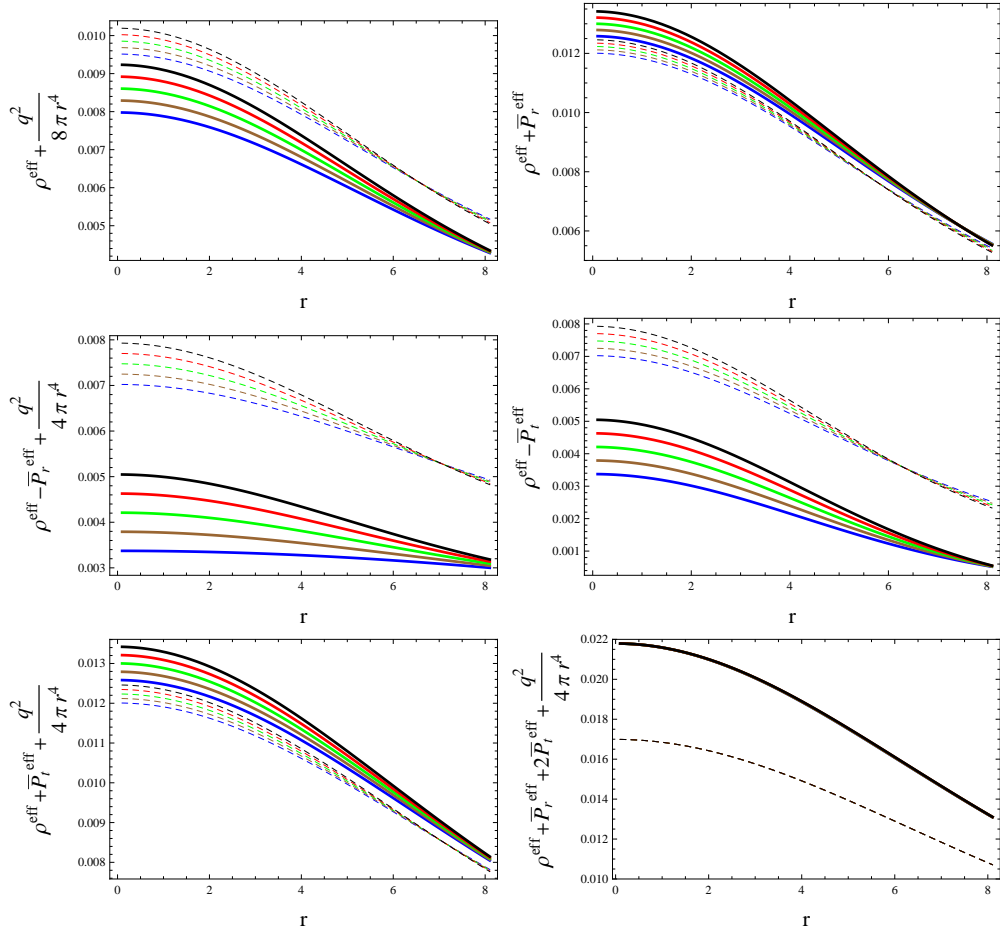


Figure 5: Plots of energy conditions versus r corresponding to $\lambda = 0.3$ (solid), 0.25 (dashed), $\delta = 0.12$ (blue), 0.14 (brown), 0.16 (green), 0.18 (red), 0.2 (black) and $Q_0 = 0.01$ for solution I.

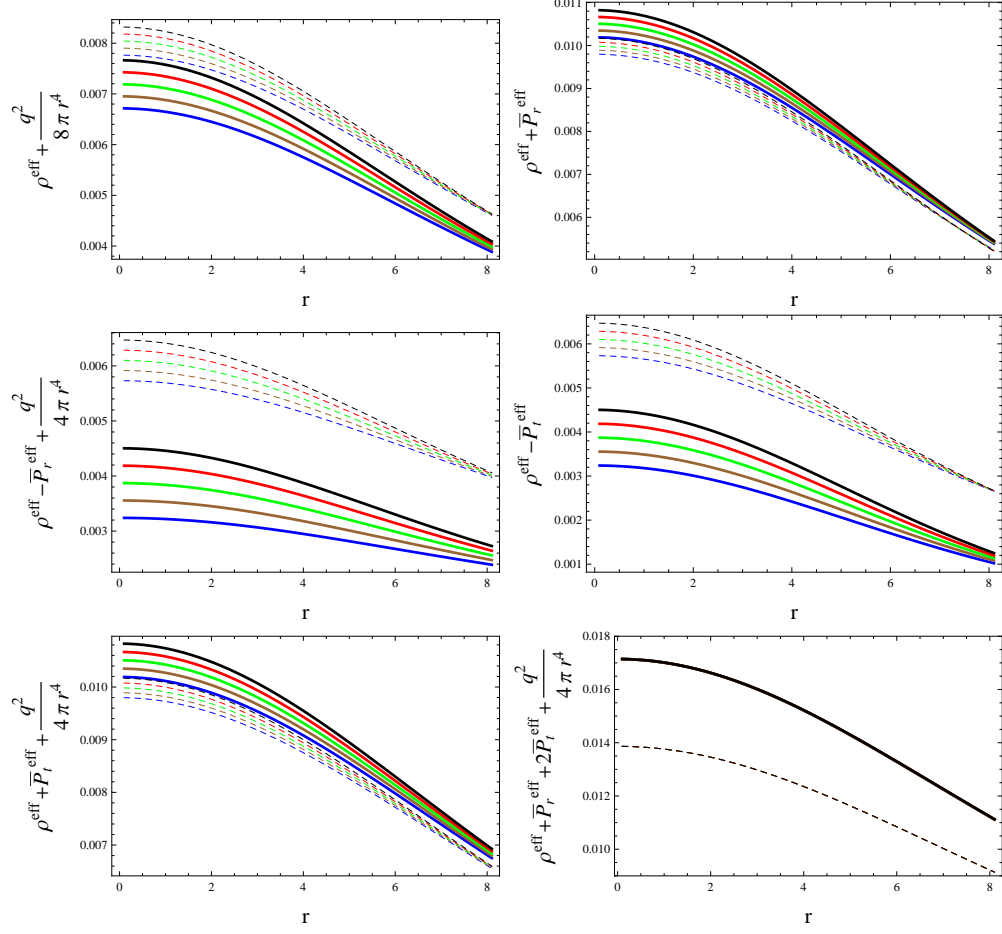


Figure 6: Plots of energy conditions versus r corresponding to $\lambda = 0.3$ (solid), 0.25 (dashed), $\delta = 0.12$ (blue), 0.14 (brown), 0.16 (green), 0.18 (red), 0.2 (black) and $Q_0 = 2$ for solution I.

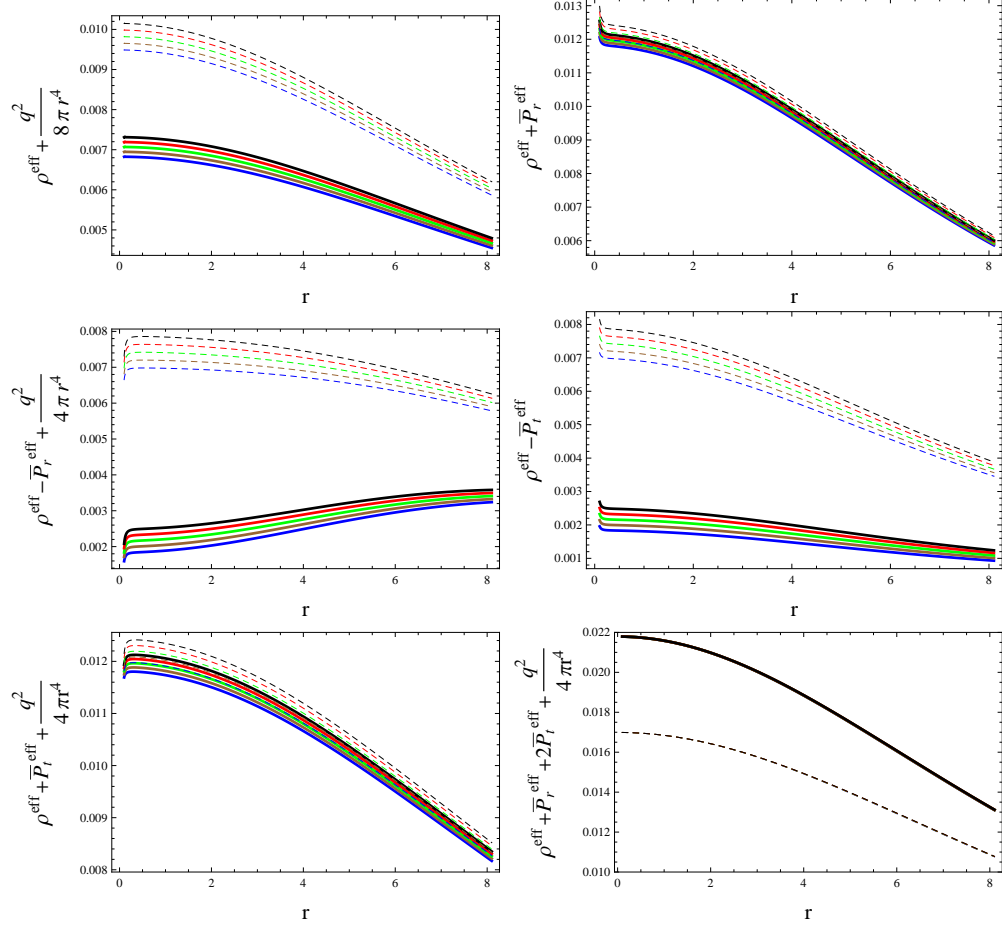


Figure 7: Plots of energy conditions versus r corresponding to $\lambda = 0.3$ (solid), 0.25 (dashed), $\delta = 0.12$ (blue), 0.14 (brown), 0.16 (green), 0.18 (red), 0.2 (black) and $Q_0 = 0.01$ for solution II.

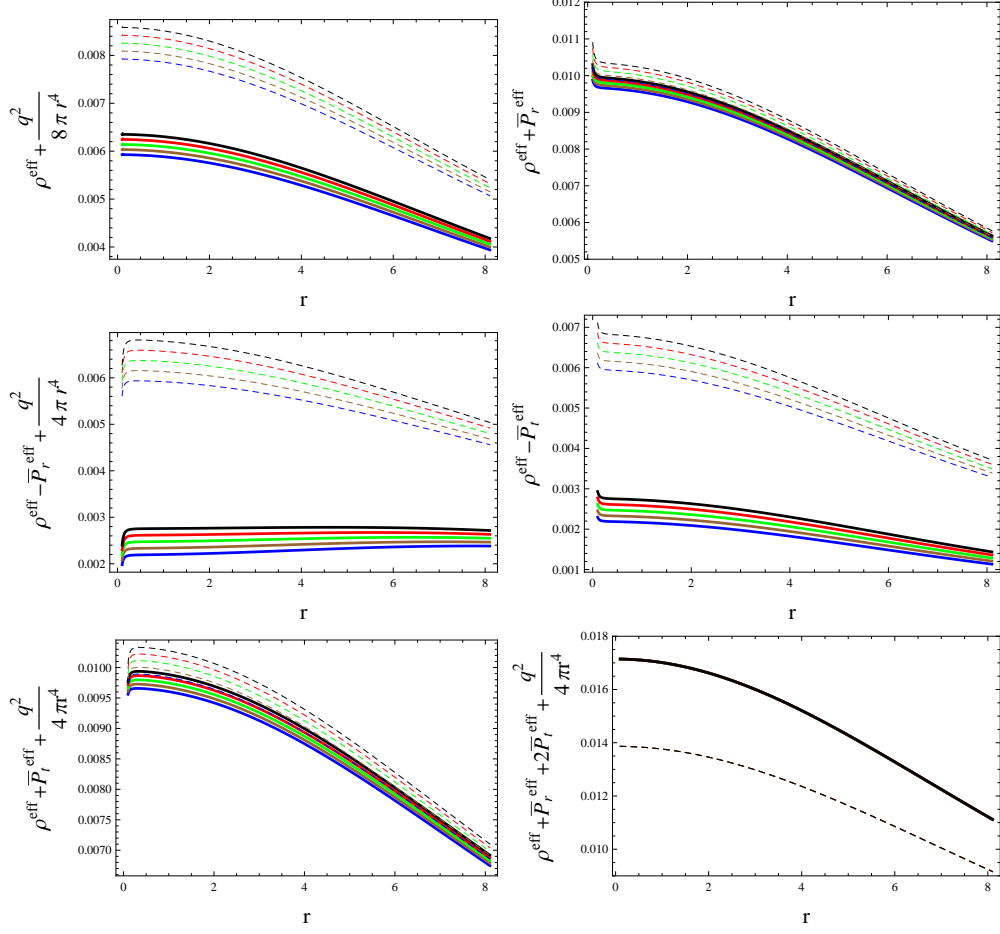


Figure 8: Plots of energy conditions versus r corresponding to $\lambda = 0.3$ (solid), 0.25 (dashed), $\delta = 0.12$ (blue), 0.14 (brown), 0.16 (green), 0.18 (red), 0.2 (black) and $Q_0 = 2$ for solution II.

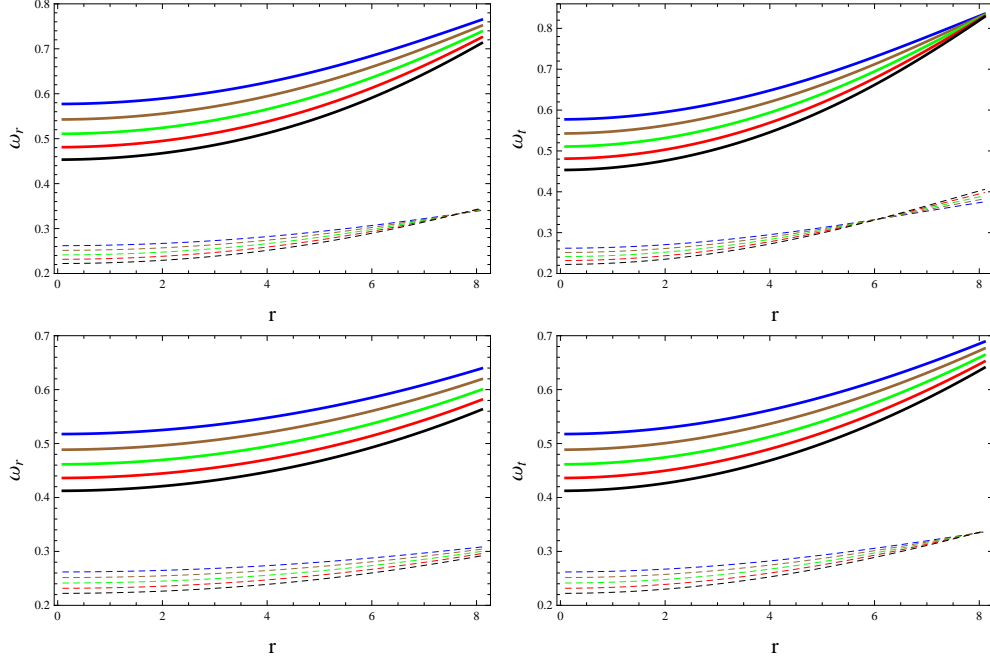


Figure 9: Plots of radial and tangential EoS parameters versus r corresponding to $\lambda = 0.3$ (solid), 0.25 (dashed), $\delta = 0.12$ (blue), 0.14 (brown), 0.16 (green), 0.18 (red), 0.2 (black), $Q_0 = 0.01$ (top row) and $Q_0 = 2$ (bottom row) for solution I

configuration, Buchdahl [43] determined the limit $u(r) < \frac{4}{9}$. The surface redshift parameter is used to evaluate the increment induced by the strong gravitational pull of a celestial body on the wavelength of electromagnetic radiations. For a perfect fluid distribution of matter, Buchdahl restricted this parameter to the limit $Z_s(r) < 2$ at the surface of the star. For an anisotropic configuration, however, the limit becomes $Z_s(r) \leq 5.211$ [44]. Figures **11** and **12** illustrate that both solutions meet the required limits for compactness and surface redshift.

Finally, to complete the physical analysis, we discuss the stability of both solutions. For this purpose, we use both the Herrera cracking approach [38] as well as the causality conditions. With the Herrera cracking technique, the stability of compact objects is implied if $0 \leq |V_{st}^2 - V_{sr}^2| \leq 1$, where $V_{st}^2 = \frac{d\bar{P}_t^{eff}}{d\rho^{eff}}$ and $V_{sr}^2 = \frac{d\bar{P}_r^{eff}}{d\rho^{eff}}$ denote the tangential and radial sound speeds, respectively.

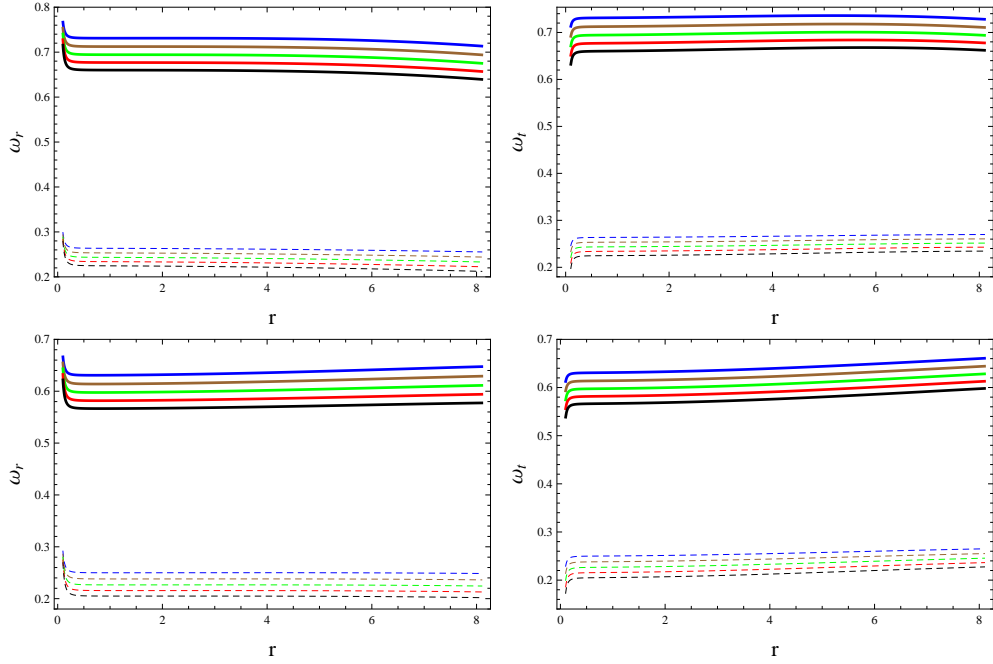


Figure 10: Plots of radial and tangential EoS parameters versus r corresponding to $\lambda = 0.3$ (solid), 0.25 (dashed), $\delta = 0.12$ (blue), 0.14 (brown), 0.16 (green), 0.18 (red), 0.2 (black), $Q_0 = 0.01$ (top row) and $Q_0 = 2$ (bottom row) for Solution II.

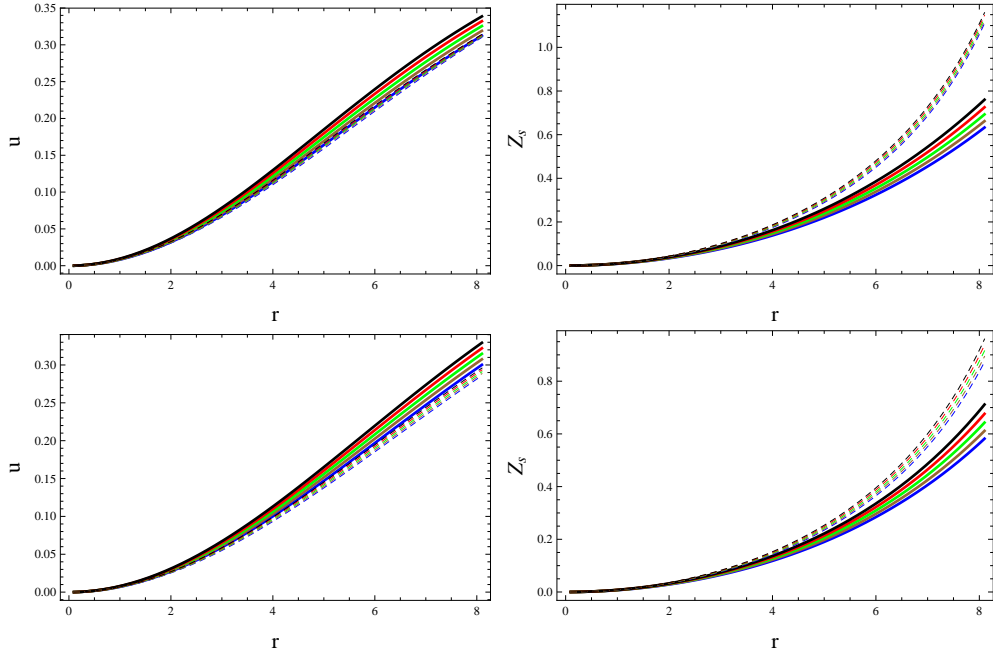


Figure 11: Plots of compactness and surface redshift versus r corresponding to $\lambda = 0.3$ (solid), 0.25 (dashed), $\delta = 0.12$ (blue), 0.14 (brown), 0.16 (green), 0.18 (red), 0.2 (black), $Q_0 = 0.01$ (top row) and $Q_0 = 2$ (bottom row) for Solution I.

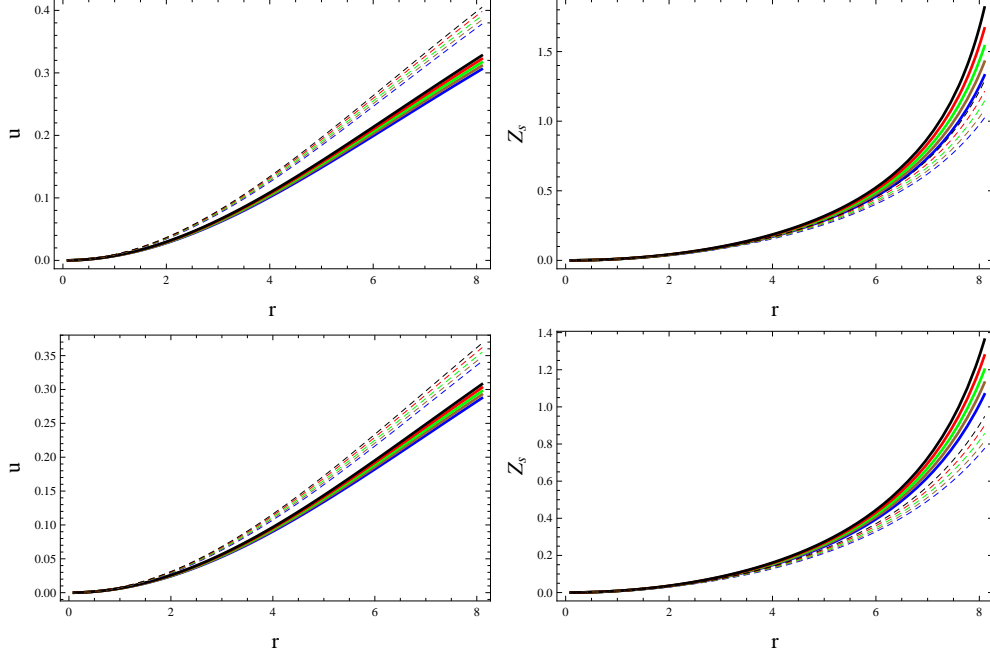


Figure 12: Plots of compactness and surface redshift versus r corresponding to $\lambda = 0.3$ (solid), 0.25 (dashed), $\delta = 0.12$ (blue), 0.14 (brown), 0.16 (green), 0.18 (red), 0.2 (black), $Q_0 = 0.01$ (top row) and $Q_0 = 2$ (bottom row) for Solution II.

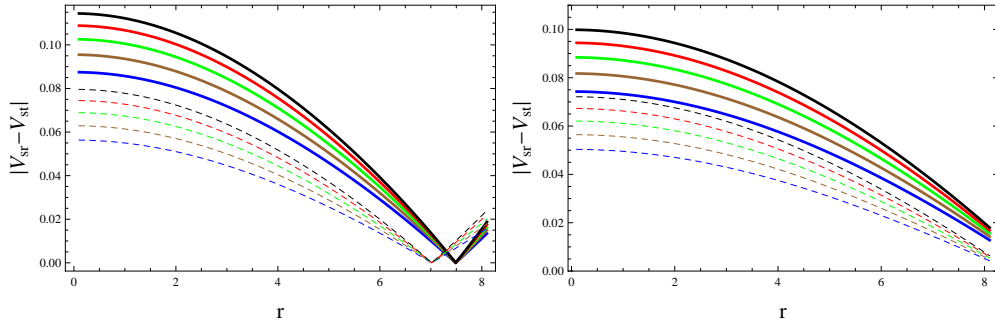


Figure 13: Plots of $|V_{st}^2 - V_{sr}^2|$ versus r corresponding to $\lambda = 0.3$ (solid), 0.25 (dashed), $\delta = 0.12$ (blue), 0.14 (brown), 0.16 (green), 0.18 (red), 0.2 (black), $Q_0 = 0.01$ (left) and $Q_0 = 2$ (right) for Solution I.

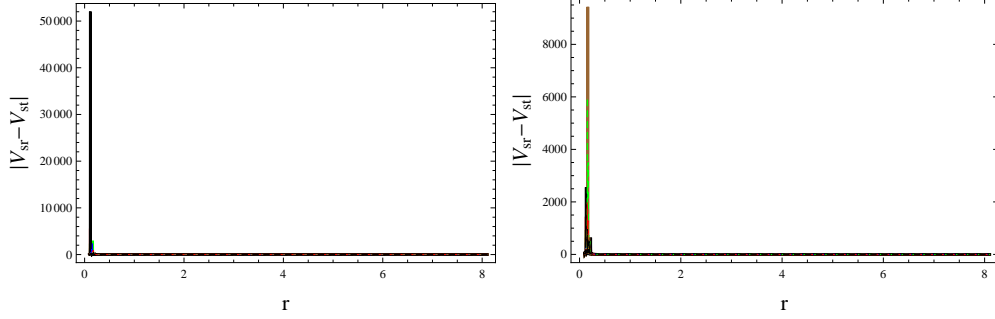


Figure 14: Plots of $|V_{st}^2 - V_{sr}^2|$ versus r corresponding to $\lambda = 0.3$ (solid), 0.25 (dashed), $\delta = 0.12$ (blue), 0.14 (brown), 0.16 (green), 0.18 (red), 0.2 (black), $Q_0 = 0.01$ (left) and $Q_0 = 2$ (right) for Solution II.

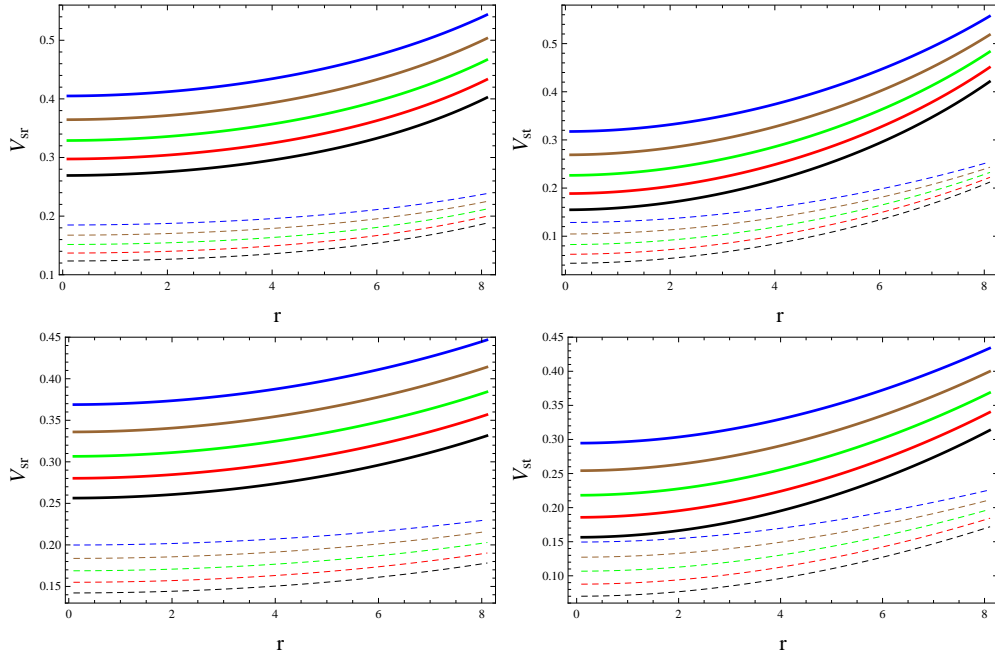


Figure 15: Plots of radial and tangential sound speeds versus r corresponding to $\lambda = 0.3$ (solid), 0.25 (dashed), $\delta = 0.12$ (blue), 0.14 (brown), 0.16 (green), 0.18 (red), 0.2 (black), $Q_0 = 0.01$ (top row) and $Q_0 = 2$ (bottom row) for Solution I.

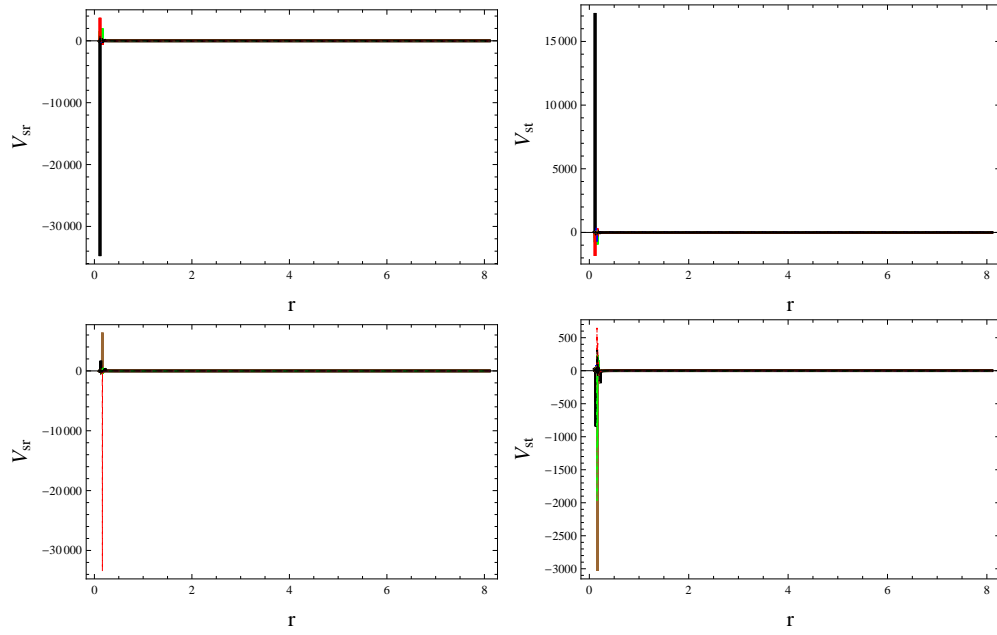


Figure 16: Plots of radial and tangential sound speeds versus r corresponding to $\lambda = 0.3$ (solid), 0.25 (dashed), $\delta = 0.12$ (blue), 0.14 (brown), 0.16 (green), 0.18 (red), 0.2 (black), $Q_0 = 0.01$ (top row) and $Q_0 = 2$ (bottom row) for Solution II.

Figures **13** and **14** show that solution I is stable for both values of the charge parameter while solution II is unstable. To further verify this result, the causality condition is employed. Here, the condition for stability is that the squared sound speed must lie in the closed interval $[0, 1]$, i.e., $0 \leq V_s^2 \leq 1$, otherwise stated, $0 \leq V_{sr}^2 \leq 1$ and $0 \leq V_{st}^2 \leq 1$. It turns out that solution I is stable while solution II is unstable as shown by the plots in Figures **15** and **16**.

5 Conclusions

In this paper, we have used gravitational decoupling through the MGD approach to explore the effects of electromagnetic field on anisotropic spherical solutions in Rastall gravity. Using this approach, the known isotropic Finch-Skea ansatz has been extended to include the effects of charge in anisotropic domain. To achieve this, we have added a new source $\Theta_{\gamma\varrho}$ to the effective charged isotropic stress-energy tensor $\bar{T}_{\gamma\varrho}^{(eff)}$, leading to the effective field equations with anisotropic distribution of matter. By deforming only the radial metric component of the known solution, the effective field equations (18)-(20) are decoupled into two sets. The first set (26)-(28) corresponds to the Rastall field equations for isotropic matter configuration while the second set (30)-(32) corresponds to the added source $\Theta_{\gamma\varrho}$. The matching conditions at the stellar surface have also been studied in detail, for an outer RN spacetime.

For the Rastall parameter $\lambda = 0.3, 0.25$ with the decoupling constant $\delta = 0.12, 0.14, 0.16, 0.18, 0.2$ and charge $Q_0 = 0.01, 2$, the physical behavior of the effective parameters $(\rho^{eff}, \bar{P}_r^{eff}, \bar{P}_t^{eff})$ and anisotropic pressure $(\bar{\Delta}^{eff})$ for both solutions have been examined. It is found that reducing the Rastall and charge parameters induces a more dense stellar interior in both solutions. However, an increment in charge coincides with a reduced compactness of stellar interior in both solutions. A rise in the decoupling parameter δ is also observed to induce a more dense interior as well as an increased anisotropy in both solutions. The generated anisotropy in both cases has been found to be positive, implying an outward directed pressure which produces the anti-gravitational force required to keep the compact object in an equilibrium state.

The physical viability of both solutions, which we have tested through graphical analysis of the energy conditions, shows that these solutions are

physically acceptable. Finally, we have discussed the stability of both solutions through two different criteria. We have found that solution I turns to be stable while solution II is unstable. It is worth mentioning here that two anisotropic solutions corresponding to a pressure-like and density-like constraint were found in GR [30]. However, only the solution corresponding to the pressure-like constraint was found to be viable and stable. Here, we have found that both solutions are viable but only the first solution is stable. We can thus conclude that more viable solutions are obtained in Rastall theory than GR.

Appendix

$$\begin{aligned}
\rho^{eff} = & \frac{C}{2\sqrt{Cr^2}(Cr^2+1)^3(2A+Br\sqrt{Cr^2})^2} \left[-(Cr^2+1) \right. \\
& \times \left(4A^2\sqrt{Cr^2}(C(4\lambda-1)r^2+12\lambda-6) - 2Br \ln \left(A + \frac{1}{2}Br\sqrt{Cr^2} \right) \right. \\
& \times \left(2B(4\lambda-1)r\sqrt{Cr^2}(Cr^2+1) \ln \left(A + \frac{1}{2}Br\sqrt{Cr^2} \right) \right. \\
& \left. \left. + 2A(C(8\lambda+1)r^2+12\lambda) + Br\sqrt{Cr^2}(3Cr^2+4\lambda+2) \right) + 4ABCr^3 \right. \\
& \times \left(C(4\lambda-1)r^2+12\lambda-6 \right) + B^2r^2\sqrt{Cr^2} \left(Cr^2(C(4\lambda-1)r^2-4\lambda-2) \right. \\
& \left. \left. - 16\lambda+4 \right) \right) + \frac{2Cr^2\delta}{\left(BCr^3 \left(4 \ln \left(A + \frac{1}{2}Br\sqrt{Cr^2} \right) + 1 \right) + 2A\sqrt{Cr^2} \right)^2} \\
& \times 16A^4\sqrt{Cr^2} \left(C^2(2\lambda-1)r^4 + 4C(\lambda-1)r^2 + 18\lambda-3 \right) + 32A^3BCr^3 \\
& \times \left(C^2(2\lambda-1)r^4 + 4C(\lambda-1)r^2 + 18\lambda-3 \right) - 8A^2B^2r^2\sqrt{Cr^2} \\
& \times \left(Cr^2(C^2(2\lambda-1)r^4 + 40C\lambda r^2 + 22\lambda-3) + 32\lambda-4 \right) + 2Br \\
& \times \ln \left(A + \frac{1}{2}Br\sqrt{Cr^2} \right) \left(Br \ln \left(A + \frac{1}{2}Br\sqrt{Cr^2} \right) \right)
\end{aligned}$$

$$\begin{aligned}
& \times \left(4A^2\sqrt{Cr^2} (Cr^2 (C(4\lambda - 11)r^2 - 8(\lambda + 1)) - 44\lambda + 3) + 4ABCr^3 \right. \\
& \times (Cr^2 (C(20\lambda - 9)r^2 + 40\lambda - 4) - 12\lambda + 5) - 4BC(4\lambda + 1)r^3 \\
& \times (Cr^2 + 1) \left(2A (Cr^2 + 3) + Br\sqrt{Cr^2} (1 - Cr^2) \right) \ln \left(A + \frac{1}{2}Br\sqrt{Cr^2} \right) \\
& \left. - B^2r^2 (Cr^2)^{3/2} (Cr^2 (C(28\lambda + 15)r^2 + 8(5\lambda + 2)) + 44\lambda + 1) \right) \\
& + 2 \left(8A^3 (Cr^2 (Cr^2 (C(1 - 2\lambda)r^2 - 14\lambda + 1) - \lambda + 3) - 9\lambda + 3) \right. \\
& - 4A^2Br\sqrt{Cr^2} (Cr^2 (Cr^2 (C(2\lambda - 1)r^2 + 16\lambda + 3) - 35\lambda - 3) + 11\lambda - 7) \\
& + 2AB^2Cr^4 (Cr^2 (Cr^2 (C(2\lambda - 1)r^2 - 14\lambda - 11) + 9\lambda - 7) - 35\lambda + 3) \\
& + B^3r^3 (Cr^2)^{3/2} (Cr^2 (Cr^2 (C(2\lambda - 1)r^2 + 4\lambda - 7) + 5\lambda - 7) - 17\lambda - 1) \left. \right) \\
& - 8AB^3Cr^5 (Cr^2 (Cr^2 (3C(2\lambda - 1)r^2 + 36\lambda - 8) + 34\lambda - 9) + 20\lambda - 4) \\
& + B^4r^4 (Cr^2)^{3/2} \left(Cr^2 (7C^2(1 - 2\lambda)r^4 + 4C(3\lambda + 5)r^2 + 90\lambda + 21) \right. \\
& \left. \left. + 48\lambda + 8 \right) \right],
\end{aligned}$$

$$\begin{aligned}
\bar{P}_r^{eff} = & \frac{C}{2\sqrt{Cr^2} (Cr^2 + 1)^2 (2A + Br\sqrt{Cr^2})^2} \left[-2\delta \left(4A^2\sqrt{Cr^2} \left(C(2\lambda - 1)r^2 \right. \right. \right. \\
& + 6\lambda - 1 \left. \right) - 2B^2(4\lambda + 1)r^2\sqrt{Cr^2} (Cr^2 + 1) 2 \ln \left(A + \frac{1}{2}Br\sqrt{Cr^2} \right) \\
& + 4Br \left(A (2C(1 - 2\lambda)r^2 - 6\lambda + 2) + Br\sqrt{Cr^2} (Cr^2 - \lambda + 1) \right) \\
& \times \ln \left(A + \frac{1}{2}Br\sqrt{Cr^2} \right) + 4ABCr^3 (C(2\lambda - 1)r^2 + 6\lambda - 1) \\
& + B^2r^2\sqrt{Cr^2} (C^2(2\lambda - 1)r^4 - C(2\lambda + 1)r^2 - 8\lambda) \left. \right) + 4A^2 \\
& \times \sqrt{Cr^2} (c(4\lambda - 1)r^2 + 12\lambda - 2) + 2Br \ln \left(A + \frac{1}{2}Br\sqrt{Cr^2} \right) \\
& \times \left(-2B(4\lambda - 1)r\sqrt{Cr^2} (Cr^2 + 1) \ln \left(A + \frac{1}{2}Br\sqrt{Cr^2} \right) \right.
\end{aligned}$$

$$\begin{aligned}
& + A \left(2C(3 - 8\lambda)r^2 - 24\lambda + 8 \right) + Br\sqrt{Cr^2} \left(Cr^2 - 4\lambda + 2 \right) \Big) \\
& + 4ABC r^3 \left(C(4\lambda - 1)r^2 + 12\lambda - 2 \right) + B^2 r^2 \sqrt{Cr^2} \left(Cr^2 \left(C(4\lambda - 1)r^2 \right. \right. \\
& \left. \left. - 4\lambda + 2 \right) - 16\lambda + 4 \right) \Big], \\
\bar{P}_t^{eff} = & \frac{C}{2\sqrt{Cr^2} (Cr^2 + 1)^3 \left(2A + Br\sqrt{Cr^2} \right)^3} \\
& \times \left[\frac{-2Cr^2\delta}{\left(4BCr^3 \ln \left(A + \frac{1}{2}Br\sqrt{Cr^2} \right) + 2A\sqrt{Cr^2} + BCr^3 \right)^2} \right. \\
& \times \left(-2AB^4 r^4 \left(C^2(10\lambda - 7)r^4 + C(6\lambda - 19)r^2 + 36\lambda - 12 \right) \right. \\
& \times (Cr^2)^{3/2} - 32A^5 \left(C(2\lambda + 1)r^2 - 6\lambda + 1 \right) \sqrt{Cr^2} - 16A^3 B^2 r^2 \\
& \times \left(3C^2(6\lambda + 1)r^4 + C(1 - 8\lambda)r^2 + 14\lambda - 2 \right) \sqrt{Cr^2} - 32B^5 C^2 r^9 \\
& \times (Cr^2 + 1)^2 (4\lambda + 1) 5 \ln \left(A + \frac{1}{2}Br\sqrt{Cr^2} \right) + 8B^4 Cr^6 (Cr^2 + 1) \\
& \times \left(BC \left(C(4\lambda + 9)r^2 - 12\lambda + 7 \right) r^3 + 2A\sqrt{Cr^2} \left(3C(1 - 12\lambda)r^2 \right. \right. \\
& \left. \left. - 52\lambda + 1 \right) \right) 4 \ln \left(A + \frac{1}{2}Br\sqrt{Cr^2} \right) + 4B^3 Cr^5 \left(B^2 C \left(4C^3(2\lambda - 1)r^6 \right. \right. \\
& \left. \left. - 3C^2(12\lambda + 7)r^4 - C(112\lambda + 25)r^2 - 84\lambda - 8 \right) r^4 + 4AB\sqrt{Cr^2} \left(4C^3 \right. \right. \\
& \times (2\lambda - 1)r^6 + 4C^2 r^4(11\lambda - 1) + C(32\lambda + 9)r^2 - 20\lambda + 9 \Big) r + 4A^2 \\
& \times \left(4C^3(2\lambda - 1)r^6 + C^2 r^4(1 - 4\lambda) + C(19 - 80\lambda)r^2 - 84\lambda + 14 \right) \Big) \\
& \times 3 \ln \left(A + \frac{1}{2}Br\sqrt{Cr^2} \right) + 2B^2 r^2 \left(2AB^2 r^2 \left(10C^3(2\lambda - 1)r^6 - 7C^2 \right. \right. \\
& \times (12\lambda + 5)r^4 + C(5 - 188\lambda)r^2 - 252\lambda + 30 \Big) (Cr^2)^{3/2} + 8A^3 \left(6C^3 r^6 \right. \\
& \times (2\lambda - 1) + C^2(36\lambda - 17)r^4 + Cr^2(36\lambda - 1) - 44\lambda + 10 \Big) \sqrt{Cr^2}
\end{aligned}$$

$$\begin{aligned}
& + B^3 C^2 r^7 \left(2C^3(2\lambda - 1)r^6 + C^2(1 - 20\lambda)r^4 + C(23 - 64\lambda)r^2 - 96\lambda \right. \\
& \left. + 20 \right) + 4A^2 B C r^3 \left(14C^3(2\lambda - 1)r^6 + C^2(132\lambda - 53)r^4 + -40\lambda + 20 \right. \\
& \left. + C(232\lambda - 19)r^2 \right) \left(2 \ln \left(A + \frac{1}{2} B r \sqrt{C r^2} \right) - 80A^4 B C r^3 \left((2\lambda + 1) \right. \right. \\
& \left. \left. \times C r^2 - 6\lambda + 1 \right) + B^5 C^2 r^9 \left(3C^2(2\lambda + 1)r^4 + c(10\lambda + 7)r^2 - 4\lambda + 4 \right) \right. \\
& \left. - 8A^2 B^3 C r^5 \left(C^2(22\lambda - 1)r^4 + C(12\lambda - 7)r^2 + 30\lambda - 6 \right) - 2B r \left(-4A \right. \right. \\
& \left. \left. \times B^3 r^3 \left(4C^3(2\lambda - 1)r^6 + C^2(4\lambda - 7)r^4 + C(8 - 3\lambda)r^2 - 55\lambda + 11 \right) (C r^2)^{3/2} \right. \right. \\
& \left. \left. + 16A^3 B r \left(C^2(8\lambda + 7)r^4 + C(4 - 43\lambda)r^2 + 5\lambda - 3 \right) \sqrt{C r^2} + B^4 C^2 r^8 \left(4C^3 r^6 \right. \right. \right. \\
& \left. \left. \times (1 - 2\lambda) + C^2(3 - 10\lambda)r^4 + 11C(2\lambda - 1)r^2 + 52\lambda - 10 \right) + 16A^4 \left(3C^2 r^4 \right. \right. \\
& \left. \left. \times (2\lambda + 1) + C r^2(1 - 16\lambda) + 6\lambda - 2 \right) - 8A^2 B^2 C r^4 \left(2C^3(2\lambda - 1)r^6 - 11C^2 \right. \right. \\
& \left. \left. \times (2\lambda + 1)r^4 + C r^2(11\lambda - 1) - 47\lambda + 8 \right) \right) \ln \left(A + \frac{1}{2} B r \sqrt{C r^2} \right) \left(\right. \\
& \left. + (C r^2 + 1) \left(2A + B r \sqrt{C r^2} \right) \left(4A^2 \sqrt{C r^2} (C(4\lambda - 1)r^2 + 12\lambda - 2) + 2B r \right. \right. \\
& \left. \left. \times \ln \left(A + \frac{1}{2} B r \sqrt{C r^2} \right) \left(-2B r \sqrt{C r^2} (4\lambda - 1) (C r^2 + 1) \ln \left(A + \frac{1}{2} B r \sqrt{C r^2} \right) \right. \right. \right. \\
& \left. \left. + A (2C(3 - 8\lambda)r^2 - 24\lambda + 8) + B r \sqrt{C r^2} (C r^2 - 4\lambda + 2) \right) + 4A B C r^3 \left(12\lambda \right. \right. \\
& \left. \left. - 2 + C r^2(4\lambda - 1) \right) + B^2 r^2 \sqrt{C r^2} \left(C r^2 (C(4\lambda - 1)r^2 - 4\lambda + 2) - 16\lambda + 4 \right) \right) \left. \right] , \\
\bar{\Delta}^{eff} &= \frac{-\delta (C r^2)^{3/2}}{(C r^2 + 1)^3 \left(B C r^3 \left(4 \ln \left(A + \frac{1}{2} B r \sqrt{C r^2} \right) + 1 \right) + 2A \sqrt{C r^2} \right)^2} \\
&\times \frac{1}{\left(2A + B r \sqrt{C r^2} \right)^3} \left[2A B^4 r^2 \left(C r^2 \left(C (5C(1 - 2\lambda)r^2 - 26\lambda + 17) r^2 \right. \right. \right.
\end{aligned}$$

$$\begin{aligned}
& + 12(\lambda + 2) \Big) - 12(\lambda - 1) \Big) (Cr^2)^{3/2} + 32A^5C \Big(C(1 - 2\lambda)r^2 - 10\lambda \\
& + 1 \Big) \sqrt{Cr^2} - 16A^3B^2 \Big(C \Big(C \Big(5C(2\lambda - 1)r^2 + 54\lambda - 7 \Big) r^2 + 14\lambda - 4 \Big) r^2 \\
& + 10\lambda - 2 \Big) \sqrt{Cr^2} - 80A^4BC^2r^3 \Big(c(2\lambda - 1)r^2 + 10\lambda - 1 \Big) + B^5C^2r^7 \\
& \times \Big(C \Big(C \Big(C(1 - 2\lambda)r^2 + 6\lambda + 5 \Big) r^2 + 20\lambda + 8 \Big) r^2 + 4(\lambda + 1) \Big) - 8A^2B^3 \\
& \times Cr^3 \Big(C \Big(C \Big(5C(2\lambda - 1)r^2 + 50\lambda - 11 \Big) r^2 + 6(3\lambda - 2) \Big) r^2 + 18\lambda - 6 \Big) \\
& + 2B \ln \Big(A + \frac{1}{2}Br\sqrt{Cr^2} \Big) \Big(- 4AB^3r^2 \Big(C \Big(C \Big(4C(2\lambda - 1)r^2 + 26\lambda - 5 \Big) \\
& \times r^2 - 21\lambda - 8 \Big) r^2 + 17\lambda - 7 \Big) (Cr^2)^{3/2} - 16A^3B \Big(C \Big(C \Big(8C(2\lambda - 1)r^2 \\
& + 66\lambda - 5 \Big) r^2 - 11\lambda + 4 \Big) r^2 - 5\lambda + 1 \Big) \sqrt{Cr^2} - 16A^4Cr \Big(C \Big(4C(2\lambda - 1)r^2 \\
& + 34\lambda - 3 \Big) r^2 - 2\lambda + 1 \Big) + B^4C^2r^7 \Big(C \Big(C(10\lambda + 3)r^2 + 20\lambda + 11 \Big) r^2 \\
& - 18\lambda + 8 \Big) - 8A^2B^2Cr^3 \Big(C \Big(C \Big(10C(2\lambda - 1)r^2 + 96\lambda - 7 \Big) r^2 + 11\lambda + 1 \Big) r^2 \\
& + 19\lambda - 2 \Big) + B \ln \Big(A + \frac{1}{2}Br\sqrt{Cr^2} \Big) \Big(- 2AB^2r^2 \Big(C \Big(2C \Big(7C(2\lambda - 1)r^2 \\
& + 84\lambda + 16 \Big) r^2 + 68\lambda + 61 \Big) r^2 + 96\lambda + 15 \Big) (Cr^2)^{3/2} - 8A^3 \Big(C \Big(2C \Big(Cr^2 \\
& \times (2\lambda - 1) - 4\lambda + 8 \Big) r^2 - 76\lambda + 23 \Big) r^2 - 8\lambda + 5 \Big) \sqrt{Cr^2} + B^3C^2r^7 \\
& \times \Big(C \Big(2C \Big(3C(1 - 2\lambda)r^2 - 8\lambda + 1 \Big) r^2 + 40\lambda + 1 \Big) r^2 - 12\lambda + 5 \Big) - 4A^2BCr^3 \\
& \times \Big(C \Big(2C \Big(5C(2\lambda - 1)r^2 - 8\lambda + 25 \Big) r^2 - 288\lambda + 85 \Big) r^2 - 84\lambda + 25 \Big) + 2BCr^3 \\
& \times \ln \Big(A + \frac{1}{2}Br\sqrt{Cr^2} \Big) \Big(B^2C \Big(Cr^2 \Big(C \Big(4C(2\lambda - 1)r^2 - 20\lambda - 33 \Big) r^2 - 64\lambda \\
& - 49 \Big) - 4(13\lambda + 5) \Big) r^4 + 4AB\sqrt{Cr^2} \Big(C \Big(4C \Big(C(2\lambda - 1)r^2 + 19\lambda - 4 \Big) r^2 \\
& + 112\lambda - 15 \Big) r^2 + 28\lambda - 3 \Big) r + 2B \Big(Cr^2 + 1 \Big) \ln \Big(A + \frac{1}{2}Br\sqrt{Cr^2} \Big)
\end{aligned}$$

$$\begin{aligned}
& \times \left(BC \left(c(20\lambda + 13)r^2 + 4\lambda + 11 \right) r^3 - 4BC \left(Cr^2 + 1 \right) (4\lambda + 1) \right. \\
& \times \ln \left(A + \frac{1}{2}Br\sqrt{Cr^2} \right) r^3 + 2A\sqrt{Cr^2} \left(C(7 - 20\lambda)r^2 - 36\lambda + 5 \right) r \\
& \left. + 4A^2 \left(C \left(C \left(4C(2\lambda - 1)r^2 + 44\lambda - 11 \right) r^2 + 32\lambda - 5 \right) r^2 - 20\lambda + 2 \right) \right) \right) \Big].
\end{aligned}$$

Data Availability: No data was used for the research described in this paper.

References

- [1] Rastall, P.: Phys. Rev. D **6**(1972)3357.
- [2] Randall, L. and Sundrum, R.: Phys. Rev. Lett. **83**(1999)3370; *ibid.* 4690
- [3] Ovalle, J.: Mod. Phys. Lett. A **23**(2008)3247.
- [4] Casadio, R., Ovalle, J. and Da Rocha, R.: Class. Quantum Grav. **32**(2015)215020.
- [5] Ovalle, J.: Int. J. Mod. Phys.: Conf. Ser. **41**(2016)1660132.
- [6] Ovalle, J. and Linares, F.: Phys. Rev. D **88**(2013)104026.
- [7] Casadio, R., Ovalle, J. and Da Rocha, R.: Class. Quantum Grav. **32**(2015)215020.
- [8] Ovalle, J.: Phys. Rev. D **95**(2017)104019.
- [9] Ovalle, J., Casadio, R., Da Rocha, R. and Sotomayor, A.: Eur. Phys. J. C **78**(2018)122.
- [10] Maurya, S.K. and Tello-Ortiz, F.: Phys. Dark Universe **29**(2020)100577.
- [11] Maurya, S.K. et al.: Phys. Dark Universe **30**(2020)100640.
- [12] Maurya, S.K. and Tello-Ortiz, F.: Phys. Dark Universe **27**(2020)100442.

- [13] Maurya, S.K. et al.: Eur. Phys. J. C **81**(2021)848.
- [14] Maurya, S.K., Tello-Ortiz, F. and Govender, M.: Fortsch. Phys. **69**(2021)2100099.
- [15] Maurya, S.K., Tello-Ortiz, F. and Ray, S.: Phys. Dark Universe **31**(2021)100753.
- [16] Sharif, M. and Saba, S.: Chin. J. Phys. **59**(2019)481.
- [17] Sharif, M. and Saba, S.: Chin. J. Phys. **63**(2020)348.
- [18] Sharif, M. and Saba, S.: Int. J. Mod. Phys. D **29**(2020)2050041.
- [19] Sharif, M. and Waseem, A.: Chin. J. Phys. **60**(2019)426.
- [20] Sharif, M. and Waseem, A.: Ann. Phys. **405**(2019)14.
- [21] Sharif, M. and Majid, A.: Chin. J. Phys. **68**(2020)406.
- [22] Sharif, M. and Majid, A.: Phys. Dark Universe **30**(2020)100610.
- [23] Xingxiang, W.: Gen. Relativ. Gravit. **19**(1978)729.
- [24] Das, B. et al.: Int. J. Mod. Phys. D **20**(2011)1675.
- [25] Sharif, M. and Bhatti, M.Z.: Astrophys. Space Sci. **347**(2013)337.
- [26] Murad, M.H.: Astrophys. Space Sci. **361**(2016)20.
- [27] Singh, K.N. and Pant, N.: Astrophys. Space Sci. **358**(2015)01.
- [28] Sharif, M. and Zeeshan Gul, M.: Eur. Phys. J. Plus **133**(2018)345.
- [29] Sharif, M. and Naz, S.: Mod. Phys. Lett. A **35**(2020)1950340.
- [30] Sharif, M. and Sadiq, S.: Eur. Phys. J. C **78**(2018)410.
- [31] Sharif, M. and Naseer, T.: Chin. J. Phys. **73**(2021)179.
- [32] Naseer, T. and Sharif, M.: Universe **8**(2022)62.
- [33] Hassan, K. and Sharif, M.: Universe **9**(2023)165.
- [34] Sharif, M. and Hassan, K.: Eur. Phys. J. Plus **137**(2022)997.

- [35] Mak, M.K., Dobson, Jr., P.N. and Harkó, T.: Int. J. Mod. Phys. D **11**(2002)207; Mak, M.K. and Harkó, T.: Proc. Roy. Soc. Lond. A **459**(2003)393.
- [36] Gleiser, M. and Dev, K.: Int. J. Mod. Phys. D **13**(2004)1389.
- [37] Sharma, R. and Maharaj, S.D.: Mon. Not. R. Astron. Soc. **375**(2007)1265.
- [38] Herrera, L.: Phys. Lett. A **165**(1992)206.
- [39] Abreu, H., Hernandez, H. and Nunez, L.A.: J. Phys.: Conf. Ser. **66**(2006)012038.
- [40] Finch, M.R. and Skea, J.E.F.: Class. Quantum Grav. **6**(1989)467.
- [41] Abubekеров, M.K., Antokhina, E.A., Cherepashchuk, A.M. and Shiman'skii, V.V.: Astron. Rep. **52**(2008)379
- [42] Shamir, M.F. and Zia, S.: Eur. Phys. J. C **77**(2017)448.
- [43] Buchdahl, H.A.: Phys. Rev. **116**(1959)1027.
- [44] Ivanov, B.V.: Phys. Rev. D **65**(2002)104011.